University of Alberta

Gauss-Chebyshev Quadratures for Wireless Performance Analysis

by

Maolin Wang

A thesis submitted to the Faculty of Graduate Studies and Research
in partial fulfillment of the requirements for the degree of

Master of Science

in

Communications

Department of Electrical and Computer Engineering

Dedicated to my beloved parents...

Abstract

Bit/symbol error rate and outage probability are common performance metrics used to quantify the reliability of wireless communication systems. Error rates for a broad class of digital modulation schemes and outage probability are expressed as integrals, which often do not have closed-form solutions. Therefore, accurate and simple approximations to develop insight are desirable. To achieve this goal, classical Gaussian Chebyshev quadrature and rational Gaussian Chebyshev quadrature rules are studied in this thesis. These rules are used to compute symbol error rates over multipath fading channels and outage caused by co-channel interference. The accuracy and convergence rate of these rules are investigated.

$\sim$

Acknowledgement

I would never have been able to finish my dissertation without the guidance of my supervisor and help from friends.

I would like to express my sincere gratitude and respect to my supervisor, Dr. Chintha Tellambura, for his excellent guidance, support and supervision. He has led me into in this promising field and offered much of his insight to a beginner as me. His advice and encouragement have been instrumental in making this work a success.

My thanks also go to the members of examining committee, Dr. Hai Jiang and Dr. Majid Khabbazian, for their time reviewing my thesis and for their valuable suggestions for improvement. I am also grateful to the faculty and the administrative staff of the ECE for their support and for creating an environment conducive to research excellence.

I would also like to thank my fellow lab-mates. It has been a pleasure to work with them, and the intellectually challenging environment they created enhanced my learning experience.

A great gratitude goes to Yamuna Dhungana, who was my co-researcher in most of the works and offered me much help. I would also like to thank Prasanna Herath and Hao Fang, who provided valuable comments on my thesis.

Finally, I would like to express my deepest gratitude and respect to my family, who gives me faithful support and great encouragement.

$\sim$

Table of Contents

List of Tables

List of Figures

List of Acronyms

GCQ — Gauss-Chebyshev Quadrature

GSM — Global System for Mobile communications

CDMA — Code Division Multiple Access

IMT — International Mobile Telecommunications

ITU — International Telecommunication Union

IEEE — Institute of Electrical and Electronics Engineers

WCDMA — Wideband CDMA

TD-SCDMA — Time Division Synchronous Coded Division Multiple Access

FOMA — Freedom of Mobile Multimedia Access

LTE — Long-Term Evolution

WLAN — Wireless Local Area Network

WPAN — Wireless Personal Area Networks

WMAN — Wireless Metropolitan Area Networks

BER — Bit Error Rate

SER — Symbol Error Rate

CCI — Co-Channel Interference

CEP — Conditional Error Probability

ASK — Amplitude Shift Keying

PSK — Phase Shift Keying

FSK — Frequency Shift Keying

QAM — Quadrature Amplitude Modulation

GMSK — Gaussian Minimum Shift Keying

CDF — Cumulative Distribution Function

PDF — Probability Density Function

AWGN	Additive White Gaussian Noise
MRC	Maximum Ratio Combining
MGF	Moment Generating Function
MAP	Maximal A Posteriori Probability
SNR	Signal to Noise Ratio

List of Symbols

$Q(x)$	Gaussian Q function
ξ	Signal energy
ξ_b	Average energy per bit
$\tilde{s}(t)$	Transmitted signal
$n(t)$	Additive white Gaussian noise
$\tilde{r}(t)$	Received signal
w_k	Quadrature weights
$J(x)$	Joukowski transformation
$p_X(x)$	Probability density function of random variable X
$\mathbb{E}(X)$	Statistical average of random variable X
$\mathbb{P}(x)$	Probability
$\varphi(x)$	Moment generating function
d	Euclidean distance
$\mathrm{Re}(X)$	Real parts of random variable X
ϵ	Error probability
γ	Signal to noise ratio
Ω	Signal to interference ratio

Chapter 1

Introduction

1.1 Wireless Communication

Due to the phenomenal growth of wireless communications in recent decades, several wireless network standards have been developed. The common ones are listed as follows [3]:

1. Global System for Mobile Communications (GSM)

   GSM, the most popular second-generation (2G) cellular standard, has dominated over 80% of the mobile phone standards by 2012 [4]. The GSM's extensions include GSM-900, GSM-1800, and GSM-1900. Data transport has been added via General Packet Radio Services (GPRS) and Enhanced Data rates for GSM Evolution (EDGE) [5].

2. Code Division Multiple Access (CDMA)

   The rival standard of GSM is CDMA, which is also referred as Interim Standard 95 (IS-95). CDMA standard has achieved a considerable subscribers base in the U.S.A. and South Korea. The CDMA family includes CDMAone, CDMA2000, and CDMA2000 1xEV.

3. International Mobile Telecommunications 2000 (IMT-2000)

   IMT-2000 refers mainly to a family of 3G standards, which have been approved by the International Telecommunication Union (ITU). The leading 3G standards include CDMA2000 and Wideband CDMA (WCDMA). The various customizations of IMT-2000 include Time Division Synchronous Coded

Division Multiple Access (TD-SCDMA) [6] and Freedom of Mobile Multimedia Access (FOMA) WCDMA [7] used China and Japan, respectively. Moreover, due to the high growth of wireless data services, Long-Term Evolution (LTE) has been developed.

4. Institute of Electrical and Electronics Engineers (IEEE) standards

These standards provide interoperability and thus have built a consensus in the communications industry. IEEE 802.11 on Wireless Local Area Network (WLAN) [8], IEEE 802.15 on Wireless Personal Area Networks (WPAN) [9], and IEEE 802.16 on Wireless Metropolitan Area Networks(WMAN) [3] are some of the most popular IEEE standards.

These wireless standards have gained widespread adaption, more than 6.8 billion mobile phone subscribers by 2013, about 96% of the world's population [10]. This strong growth is facilitated and governed by the abovementioned wireless standards. Bit error rate (BER) targets and modulation schemes for these standards are listed in Table 1.1.

Table 1.1: Typical wireless telecommunication standards

Group	Standard	Modulation	Maximum Allowed BER
GSM	GSM900/GSM1800/GSM1900	Gaussian Minimum Shift Keying (GMSK)/ Quadrature Amplitude Modulation (QAM)	10^{-5} [11]
	EDGE	8 Phase Shift Keying (8PSK)	
CDMA/IMT-2000	CDMAone	Quadrature Phase Shift Keying (QPSK)	10^{-4} [12]
	CDMA2000	QPSK/8PSK/16QAM	
	TD-SCDMA	QPSK/8PSK/16QAM	
IEEE	802.11 (WLAN)	PSK/QAM	8×10^{-8} [13]
	802.15 (WPAN)	Amplitude Shift Keying (ASK)/Frequency Shift Keying (FSK)/PSK	10^{-7} [9]
	802.16 (WMAN)	PSK/QAM	10^{-6} [14]

The BER is the ratio of the number of error bits to the total number of transmitted bits during a certain time interval, and is perhaps the most important quality of service (QoS) measure. It provides a useful method to quantify the reliability of wireless channels for different wireless standards and modulation schemes. For example, for QAM in GSM900/GSM1800/GSM1900 and IEEE 802.11 (WLAN), the

maximal allowed BER differs. As a result, for each standard to maintain a reliable transmission, the BER due to the difference between the received and transmitted signals influenced by noise, interference, and fading through the channels is specified.

BER is closely related to symbol error rate (SER), which is the ratio between the number of erroneously decoded symbols and the total number of transmitted symbols. For binary modulations, the BER is simply equal to the SER. For M-ary modulation, however, since one symbol represents $\log_2 M$ bits, BER and SER may be roughly related as

$$\text{BER} \simeq \frac{1}{\log_2 M}\text{SER}. \tag{1.1}$$

Due to this relationship, SER serves as a simple proxy for BER. This thesis therefore investigates accurate SER evaluations of several digital modulation schemes used in the aforementioned wireless standards (Table 1.1). Since these wireless systems operate over multipath fading channels, which are the fundamental cause of harmful signal-strength fluctuations and result in increasing the SER, accurate evaluation of SER reveals the BER degradation due to fading.

Wireless performance also degrades due to co-channel interference (CCI), which arises when multiple users access the same time-frequency slots. The impact of CCI can be measured in terms of the outage probability. Thus, this thesis also studies the outage probability of wireless systems due to CCI.

1.2 Problem Statement

As mentioned in Section 1.1, BER/SER, outage and capacity are used to quantify wireless system performance. These metrics can be expressed in the following generalized format as [15, 16]

$$\mathbb{E}[h(x)] = \int_0^\infty h(\eta\gamma)p_\gamma(\gamma)\,d\gamma, \tag{1.2}$$

where $h(.)$ represents outage, BER/SER, or capacity; η is a parameter dependent on different types of measures; and γ is the instantaneous signal to noise ratio (SNR) or signal to interference ratio (SIR). The average is performed over the probability

density function (PDF) of γ, $p_\gamma(\gamma)$. Further details of (1.2) can be found in Table 2.1.

However, obtaining the exact closed-form for (1.2) either may not always be possible or may have a high computation complexity and may not give the direct insight about the core parameters that dominate the performance. Therefore, accurate and simple approximations to develop insight are desirable.

Specifically, two Gaussian Chebyshev quadrature (GCQ) rules are studied in this thesis to tackle these problems.

- Gaussian quadrature allows approximate evaluation of integrals (1.2) as a simple weighted sum. GCQ rules are special cases of Gaussian quadrature, which have been widely used in numerical analysis for approximation calculations.

- Specifically, GCQ rules for SER and outage analysis have been studied extensively. While classical GCQ rule is commonly used for wireless analysis, the accuracy of this rule has not been investigated in detail. However, it is known that in the high SNR region, the classical GCQ rule is highly accurate. What is not known widely is that the GCQ rule requires a large number of terms for the low SNR region. Thus, the convergence rate of this rule depends on the operating SNR. In this thesis, the convergence rates in both low and high SNR regions are investigated.

- Moreover, rational GCQ, which has not yet been widely used, is also studied in this thesis. Rational GCQ rule for SER of several digital modulations and outage probability is comprehensively described. Furthermore, SER expressions of digital modulations amenable to GCQ rules are tabulated. Also, rational GCQ rule for outage computation is developed.

- The comparisons of the convergence rates of classical GCQ and rational GCQ rules have been paid little attention. Thus, the convergence rate, measured by the minimum required numbers of nodes for each GCQ rule, for SER and outage probability is investigated in this thesis.

1.3 Contributions and Outline

The main contributions of the thesis are assessment and comparison of the accuracy of classical and rational GCQ rules for SER of several digital modulation schemes and for wireless outage. These contributions are listed below:

- SER expressions for coherent and noncoherent digital modulations that can use the GCQ rules are presented.

- Both classical and rational GCQ rules to approximate SER of wireless transmissions over multipath fading channels, Rayleigh, Rician and Nakagami-m, are presented. Their convergence rates are compared by evaluating the number of nodes needed to achieve a given level of accuracy.

- A Gaussian integral model for arbitrary upper limits for M-ary PSK modulation is developed by using the rational GCQ rule. Expression of error probability of M-PSK modulation, using the rational GCQ rule, is analyzed instead of using the former analysis with Gaussian Q-function in the format of Craig's transformation with limit $[0, \pi/2]$.

- Rational GCQ rule is adopted for outage analysis of several cases, which are a desired Rician faded signal and aggregate CCI under Rayleigh or Rician or the combination of these two fading scenarios. Convergence rate is studied through the number of nodes required for a given accuracy level.

The thesis has the following organization:

Chapter 2

In Chapter 2, basic background concepts and models of digital modulation schemes are presented. Mathematical tools of the classical and rational GCQ rules and node and weight computation are also described.

Chapter 3

Chapter 3 reviews error performance of coherent and noncoherent digital modulations. Multipath fading models are presented, and the conditional error probability

(CEP) of each modulation is obtained. Subsequently, classical and rational GCQ rules for calculating SER are evaluated. Numerical performance results for digital modulation and diversity schemes are presented.

Chapter 4

Chapter 4 investigates classical and rational GCQ rules for CCI outage. The exact closed-form outage expressions in the generalized fading scenario are derived. Numerical results of the desired signal under the Rician fading in the presence of multiple CCI is presented.

Chapter 5

Finally, Chapter 5 concludes the thesis and provides directions for further research.

$\sim$

Chapter 2

Background

This chapter describes several digital modulation schemes and mathematical tools and methods that are used for their performance analyses. Specifically, Gaussian Q-function and GCQ rules are discussed.

2.1 Digital Modulation
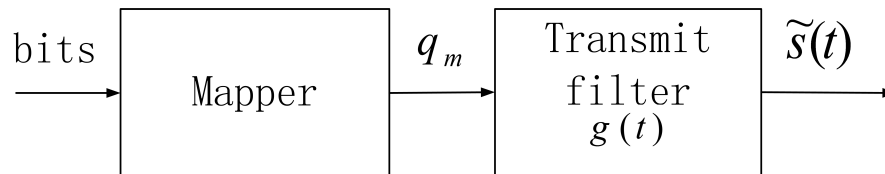
Figure 2.1: Digital modulator

A typical digital modulator (Figure 2.1) maps input digital bits to a sequence of real or complex symbols, q_m, where $m = 1, 2, ..., \infty$. Modulated symbol q_m may be expressed as

$$q_m = \begin{cases} a_m & \text{amplitude modulation} \\ e^{j\theta_m} & \text{phase modulation} \\ e^{j2\pi f_m t} & \text{frequency modulation} \end{cases} \tag{2.1}$$

where $j = \sqrt{-1}$, and a_m, θ_m, and f_m are amplitude, phase, and frequency terms, respectively. These terms are functions of input data bits. How inputs are mapped to a_m, θ_m, and f_m is determined by the given modulation scheme. The stream of q_m ($m = 1, 2, ..., \infty$) drives a transmit filter whose output is $\tilde{s}(t)$.

The modulated signal may then be expressed as

$$\tilde{s}(t) = \sum_{m=-\infty}^{+\infty} a_m g(t - mT_s), \tag{2.2}$$

where a_m is the information amplitude in the mth symbol interval, and $g(t)$ is the pulse shape of the transmit filter with duration T_s seconds.

The baseband modulated signal $\tilde{s}(t)$ is transmitted over a wireless channel by using a suitable carrier. For our purposes, the transmit signal energy and d_{min}, the minimum Euclidean distance between any two constellation points, are the critical parameters. These parameters for several modulations will be presented next.

2.1.1 ASK

Since ASK simply maps input digital data to the amplitude of the carrier signal, its mapper output thus takes on symmetric real values from

$$a_m = 2m - 1 - M, \ m = 1, 2, \ldots, M. \tag{2.3}$$

Hence, the amplitudes are $\pm 1, \pm 3, \ldots, \pm(M - 1)$ in each symbol duration T_s. Since $\log_2 M$ is the number of bits per symbol, the bit duration is given by $T_b = T_s / \log_2 M$.

If ξ_g is the energy of $g(t)$, the transmit signal energy is given by [1]

$$\begin{aligned} \xi_{avg} &= \frac{\xi_g}{2M} \sum_{m=1}^{M} a_m^2 \\ &= \frac{2\xi_g}{2M} (1^2 + 3^2 + \ldots + (M - 1)^2) \\ &= \frac{(M^2 - 1)\xi_g}{6}. \end{aligned}$$

Since energy consumption for data transmission is a critical factor, the energy per bit $\xi_{b,avg} = \xi_{avg} / \log_2 M$ is important. The energy per bit is given by [1]

$$\xi_{b,avg} = \frac{(M^2 - 1)\xi_g}{6 \cdot \log_2 M}. \tag{2.4}$$

For notational simplicity, $\xi_{b,avg}$ is represented as ξ_b.

Three ASK signal constellations are shown in Figure 2.2.

(a) BASK ($M = 2$)

0   1

(b) 4-ASK ($M = 4$)

00   01   11   10

(c) 8-ASK ($M = 8$)

000   001   011   010   110   111   101   100
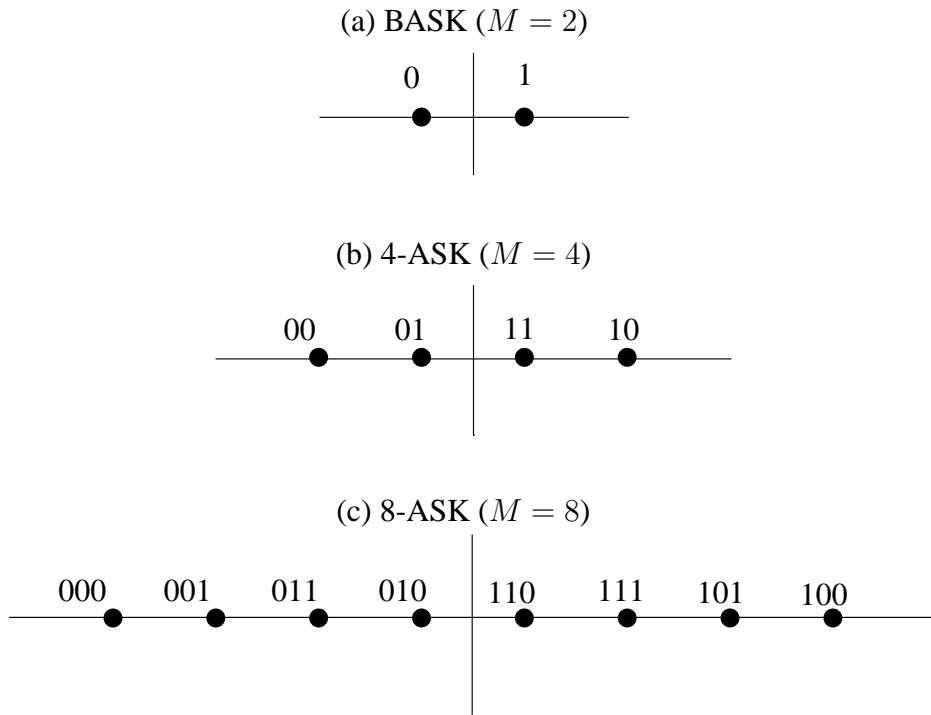
Figure 2.2: ASK Constellation [1]

The minimum distance of two constellation points is thus given by [1]

$$d_{min} = \sqrt{2\xi_g}. \tag{2.5}$$

The minimum ASK distance can be expressed in terms of ξ_b by substituting (2.4) into (2.5). Thus, in terms of the constellation size and energy per bit, the minimum distance becomes [1]

$$d_{min} = \sqrt{\frac{12\log_2 M}{M^2 - 1}\xi_b}. \tag{2.6}$$

The minimum distance is critical to the operation of the detector, which searches among all possible transmitted signal points to find the one that is closest to the received signal in terms of the Euclidean distance. In Chapter 3, error probability of ASK will be described in terms of d_{min}.

ASK is commonly used to transmit data in optical fibres and has the advantage of simple implementation. But it is an inefficient modulation technique since it is highly susceptible to noise interference, such as atmospheric and impulse noises,

9

which tend to cause rapid fluctuations in amplitude [17]. These drawbacks are eliminated in PSK and QAM, which will be discussed next.

2.1.2 PSK

In PSK, information bits drive the phase of the carrier signal. The phase signal $\theta(t)$ thus takes values from the discrete set

$$\theta_m = \frac{2\pi(m-1)}{M}, \ m = 1, 2, \ldots, M \tag{2.7}$$

in each symbol duration T_s.

Since phase change does not affect the signal energy, the relationship between energy per bit and signal energy is

$$\xi_b = \frac{\xi_g}{2\log_2 M}. \tag{2.8}$$

Transmitted PSK signal can be represented as [1]

$$\begin{aligned}
\tilde{s}(t) &= \mathrm{Re}[e^{j\theta_m} \cdot g(t) \cdot e^{j2\pi f_c t}] \\
&= \mathrm{Re}[e^{j\frac{2\pi(m-1)}{M}} \cdot g(t) \cdot e^{j2\pi f_c t}] \\
&= g(t)\cos(\frac{2\pi(m-1)}{M})\cos(2\pi f_c t) - g(t)\sin(\frac{2\pi(m-1)}{M})\sin(2\pi f_c t). \tag{2.9}
\end{aligned}$$

where $m = 1, 2, ..., M$ is the M possible phases of the carrier that convey the transmitted information, and f_c is the carrier frequency.

Binary PSK (BPSK, $M = 2$), quaternary PSK (QPSK, $M = 4$), and 8-PSK signal constellations are shown in Figure 2.3. Note that constellation points are uniformly spaced by $2\pi/M$ radians on a unit circle.

The Euclidean distance between two signal points is [1]

$$\begin{aligned}
d_{mn} &= \sqrt{||s_m - s_n||^2} \\
&= \sqrt{\xi_g[1 - \cos(\frac{2\pi}{M}(m-n))]}. \tag{2.10}
\end{aligned}$$

Therefore, the minimum distance of the constellation can be found to $|m - n| = 1$ is [1]

$$d_{min} = \sqrt{\xi_g(1 - \cos\frac{2\pi}{M})} = \sqrt{2\xi_g(\sin^2\frac{2\pi}{M})}. \tag{2.11}$$

10

(a) BPSK ($M = 2$)   (b) QPSK ($M = 4$)   (c) Octal PSK ($M = 8$)
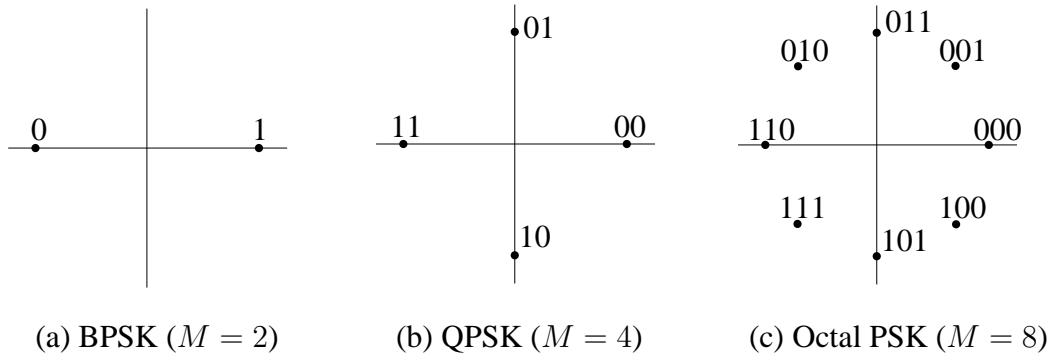
Figure 2.3: PSK Constellation [1]

With simple modification and by substituting (2.8) into (2.11), d_{min} in terms of ξ_b can be expressed as [1]

$$d_{min} = 2\sqrt{(\sin^2 \frac{\pi}{M} \times \log_2 M)\xi_b}. \tag{2.12}$$

As described previously, the key factor for the detector reliability is d_{min}, which will be discussed for PSK error probabilities in Chapter 3.

PSK is used for high-speed data transfer applications [17]. The outstanding feature of PSK is that it is more robust against the interference than ASK. However, PSK modulation requires more complex signal detection and recovery processes.

2.1.3 QAM

QAM can be viewed as a combination of amplitude/phase modulation. The two separate in-phase and quadrature carriers are in the form of $\cos(2\pi f_c t)$ and $\sin(2\pi f_c t)$, which are separated by a phase shift of $\pi/2$ radians. The QAM signal may be expressed as [1]

$$\tilde{s}(t) = \mathrm{Re}[(a_{mi} + ja_{mq})g(t)e^{j(2\pi f_c t)}]$$
$$= a_{mi}g(t)\cos(2\pi f_c) - a_{mq}g(t)\sin(2\pi f_c), \tag{2.13}$$

where the in-phase and quadrature-phase carriers are modulated by the information bearing amplitudes a_{mi} and a_{mq}. These are usually independently distributed over the set of equiprobable values

$$a_{mi}, a_{mq} \in \{2i - 1 - \sqrt{M} | i = 1, 2, \ldots, \sqrt{M}\}.$$

11

The transmit signal energy is the sum of in-phase and quadrature-phase terms:

$$\xi_m = \frac{a_{mi}^2}{2} \cdot \xi_g + \frac{a_{mq}^2}{2} \cdot \xi_g. \tag{2.14}$$

In Figure 2.4, M-ary QAM signal constellations where M is a power of two are presented; i.e., $M = 2^k$, such as $M = 4, 16, 64$, and with amplitudes $\pm 1, \pm 3, \dots,$ $\pm(\sqrt{M} - 1)$ on both horizontal and vertical directions. An immediate observation is that when k is the integral power of 2, the constellations are rectangular.
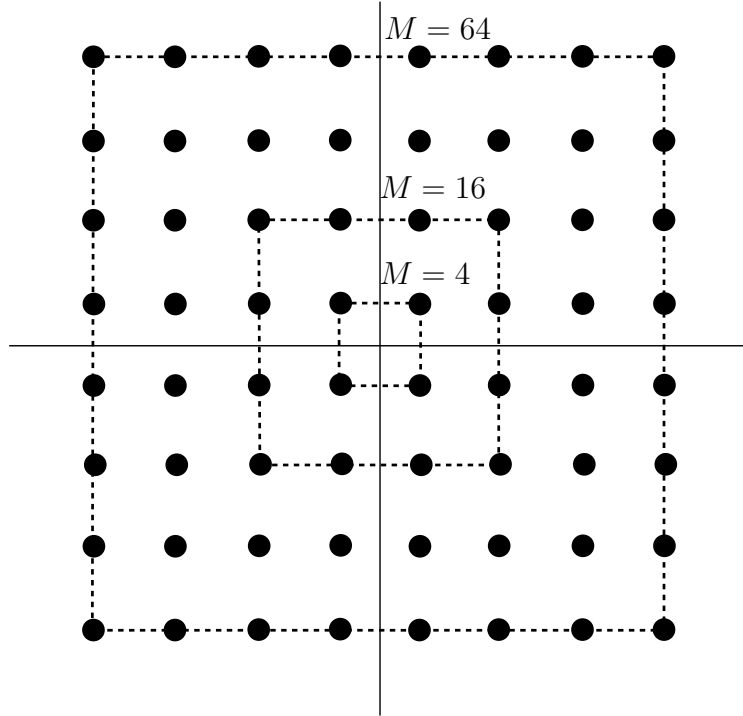
Figure 2.4: QAM Constellation [1]

The Euclidean distance between a pair of QAM points is [1]

$$d_{mn} = \sqrt{||s_m - s_n||^2}$$
$$= \sqrt{\left(\frac{a_{mi}^2 - a_{ni}^2}{2} + \frac{a_{mq}^2 - a_{nq}^2}{2} \right) \xi_g}. \tag{2.15}$$

Since the constellation map is a rectangular gird with points uniformly spaced along each axis by 2 units, the minimum distance is

$$d_{min} = \sqrt{2\xi_g}. \tag{2.16}$$

For the squared QAM modulation, the average signal energy and energy per bit are [1]

$$\xi = \frac{\xi_g}{2 \cdot M} \sum_{m=1}^{\sqrt{M}} \sum_{n=1}^{\sqrt{M}} (a_m^2 + a_n^2)$$

$$= \frac{\xi_g}{2 \cdot M} \times \frac{2M(M-1)}{3} = \frac{(M-1)\xi_g}{3}, \tag{2.17}$$

$$\xi_b = \frac{\xi}{\log_2 M} = \frac{(M-1)\xi_g}{3\log_2 M}, \text{ respectively.} \tag{2.18}$$

The minimum distance in terms of ξ_b is then given by [1]

$$d_{min} = \sqrt{\frac{6\log_2 M}{M-1}}\xi_b, \tag{2.19}$$

where d_{min} once again is the critical parameter when the detector searches among all possible transmitted signals to find the one that is closest to the received signal. The QAM error probability will be discussed in Chapter 3.

QAM modulation is widely used in cable TV, Wireless Fidelity (Wi-Fi), and WLAN to achieve high data rates over bandwidth-limited channels. For example, the most generally used 64-QAM can reach up to 54 Mbit/s in the WLAN of 2.4 GHz frequency band [17]. The advantage of QAM modulation is the enormous efficiency of spectrum usage since it contains two independent carrier signals. For example, the theoretical spectrum efficiency of 64-QAM can reach up to 6 bits/s/Hz. However, demodulation, especially in the presence of noise, can be challenging.

2.1.4 FSK

FSK encodes the input information bits in the frequency of the carrier. The frequencies thus take values from

$$f_m = \frac{(2m-1)\pi}{M}, \ m = 1, 2, \ldots, M \tag{2.20}$$

in each symbol interval T_s. Therefore, $f(t)$ can be modelled in the form of

$$f(t) = \sum_{m=-\infty}^{+\infty} f_m g(t - mT_s), \tag{2.21}$$

where f_m is the information frequency for the mth symbol, and $g(t)$ is a unit amplitude rectangular pulse of duration T_s.

In contrast to ASK and PSK, FSK is multidimensional signalling due to the multiple carrier frequencies. In fact, FSK is a special case of *orthogonal modulation*, in which the signal set is mutually orthogonal and has equal energy, such that [1]

$$\int_{-\infty}^{\infty} \tilde{s}_m(t)\tilde{s}_n(t)\,dt = \begin{cases} \xi & m = n \\ 0 & m \neq n \end{cases}$$

For $M = 3$, these symbols are represented in Figure 2.5.
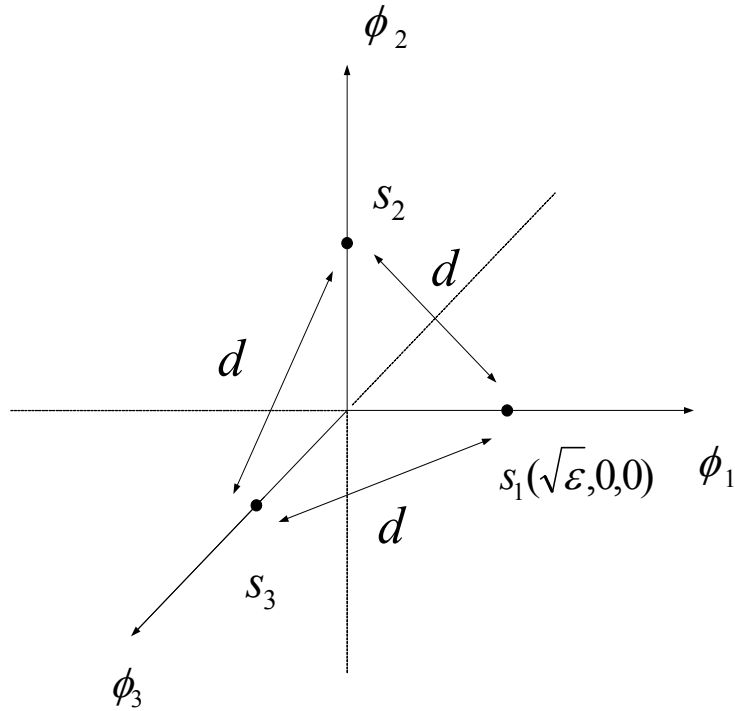
Figure 2.5: 3-FSK Constellations [1]

The minimum Euclidean distance is

$$d_{min} = \sqrt{2\xi}. \tag{2.22}$$

The relationship between average energy per symbol and energy per bit is given by

$$\xi_b = \frac{\xi}{\log_2 M}. \tag{2.23}$$

The minimum distance can be expressed as [1]

$$d_{min} = \sqrt{2\log_2 M \cdot \xi_b}. \tag{2.24}$$

Error Probability of FSK will be discussed in detail in Chapter 3.

14

2.2 Performance Integrals

As stated in Section 1.2, typical wireless performance metrics, such as BER/SER, capacity, and outage can be expressed as integrals. For convenience, we repeat (1.2) here again as

$$\mathbb{E}[h(x)] = \int_0^\infty h(\eta\gamma)p_\gamma(\gamma)\,d\gamma. \tag{2.25}$$

Several cases chosen for $h(x)$ are listed in Table 2.1.

Table 2.1: Common performance measures

Expression type	$h(\gamma)$
SER	$Q(\sqrt{\alpha\gamma})$
Outage	$\mathbb{P}[\gamma < \gamma_{th}]$
Capacity	$\log_2(1+\gamma)$

For SER, only the case of BPSK is listed, where $\alpha = 2$, γ is the instantaneous SNR, and $Q(.)$ is Gaussian Q-function described in the next section. The SER of most coherent modulations can be represented by $Q(.)$ or linear combination of weighted $Q(.)$'s or powers of $Q(.)$. For outage, γ_{th} is the power protection ratio or minimum receiver SIR requirement, usually $\gamma_{th} = 9.5$ dB [18]. The capacity is given by the classical Shannon formula.

The performance measures given in Table 2.1 and (2.25) can be easily computed by using the Gaussian quadrature rules. In this thesis, two specific numerical estimations achieved by using the Gaussian quadrature, classical and rational GCQ rules, are considered. Those methods will be further adopted for error and outage performance analysis in the following chapter.

Next, Gaussian Q-function is introduced. Classical and rational GCQ rules are discussed later.

2.3 Gaussian Q-Function

Gaussian Q-function or equivalently the complementary error function erfc($\cdot$) is often used for performance analysis. This is due to the fact that conditional BER/SER of a broad class of coherent and differentially encoded digital modulation schemes

15

can be expressed in terms of Q-function [1, 19]. A detailed list of conditional BER/SER expressions involving Q-function is given in Table 3.1. The Gaussian Q-function is defined as the complement of the cumulative distribution function (CDF) of a zero mean and unit variance Gaussian random variable. The canonical representation of Gaussian Q-function can be expressed as

$$Q(x) = \frac{1}{2}\text{erfc}(\frac{x}{\sqrt{2}}) = \int_x^\infty \frac{1}{\sqrt{2\pi}}\exp(-\frac{y^2}{2})\, dy, x \geq 0. \tag{2.26}$$

This form presents analytical difficulties for numerical integral evaluation since the lower limit of $Q(x)$ contains x, and the upper limit is infinity. This is due to the fact that in order to calculate the average error rate, (2.26) needs to be averaged over the PDF of random variable x. For such cases, variable x present in the lower integration limit is a drawback. Therefore, various approximations, bounds and expressions have been derived for solving this issue [20–30]. Craig [31] generates one such closed-expression for the Gaussian Q-function, which can be written as

$$Q(x) = \frac{1}{\pi}\int_0^{\pi/2} \exp\left(-\frac{x^2}{2\sin^2\theta}\right)\, d\theta, \tag{2.27}$$

$$Q^2(x) = \frac{1}{\pi}\int_0^{\pi/4} \exp\left(-\frac{x^2}{2\sin^2\theta}\right)\, d\theta. \tag{2.28}$$

Expressions (2.27) and (2.28) have finite integration limits independent of the argument x. These forms are particularly useful in the analysis of the error rates of coherent and noncoherent modulation schemes in the presence of fading, which will be presented in Chapter 3. Moreover, to evaluate error probability efficiently and precisely, Gaussian quadrature is described next.

2.4 Gaussian Quadrature

Gaussian quadrature has been widely used in numerical analysis for approximation calculation of definite integrals. For a definite integral $f(x)$, [32]

$$I(f) = \int_a^b f(x)u(x)\, dx. \tag{2.29}$$

an m-point Gaussian quadrature rule may be expressed as

$$I_m(f) = \sum_{k=1}^{m} w_k f(x_k) + R_m, \qquad (2.30)$$

where x_k are the quadrature points which depend on the number of nodes m but not on $f(x)$, w_k are the quadrature weights, and $u(x)$ is a weight function on $[a, b]$, where a and b are normally set to -1 and 1, respectively. The R_m is the remainder or error term. Its key idea is to use the interpolation nodes in range $[a, b]$ to maximize the exactness and accuracy. The use of Gaussian quadrature has been found to be convenient for wireless analysis.

2.4.1 Classical GCQ

The classical GCQ was first introduced by Bigilier, Caire, Taricco and Ventura-Travest in [33] and [34]. This method was further developed for error performance analysis of coded system in [35, 36], diversity combing systems with binary modulations in [37], and M-ary quadrature amplitude modulation (M-ary QAM) in [38]. The classical GCQ technique is simple and useful, but it requires a higher number of nodes for accurate results in low SNR.

The classical GCQ rule can be expressed as the special case of (2.29) when $a = -1$, $b = 1$, and $u(x) = 1/\sqrt{1-x^2}$. For this case, nodes and weights are explicitly given. This rule can be given as [39]

$$\int_{-1}^{+1} \frac{f(x)}{\sqrt{1-x^2}} \, dx = \sum_{k=1}^{m} \omega_k f(x_k) + R_m, \qquad (2.31)$$

where $\omega_k = \pi/m$ and $x_k = \cos(2k-1)\pi/2m$ are the corresponding weights and nodes. In (2.31), the integral is approximated by the summation of the weighted values of $f(x)$ evaluated at the abscissas x_k, where $k = 1, 2, \ldots, m$. It can be shown that the error $R_m = 0$ if $f(x)$ is a polynomial of a degree less than or equal to $2m - 1$ [40].

2.4.2 Convergence of classical GCQ

Convergence refers to how fast $|R_m| \to 0$ as m increases. To explore classical GCQ rule's convergence rate, Cauchy integral in the complex plane is advocated [41]. If

17

function $f(x)$ is analytic in a domain containing $[-1, 1]$, Cauchy's integral formula for $I(f)$ can be expressed as

$$\begin{aligned}
I(f) &= \int_{-1}^{+1} \frac{f(x)}{\sqrt{1-x^2}}\, dx \\
&= \int_{-1}^{+1} \frac{1}{2\pi i} \int_\Gamma \frac{f(z)}{\sqrt{1-x^2}(z-x)}\, dz\, dx \\
&= \frac{1}{2\pi i} \int_\Gamma f(z)\phi(z)\, dz,
\end{aligned} \tag{2.32}$$

where Γ is a contour contained in the domain of analyticity of f that encloses $[-1, 1]$ once in the counter-clockwise direction, and $\phi(z)$ is given by

$$\phi(z) = \int_{-1}^{+1} \frac{1}{\sqrt{1-x^2}(z-x)}\, dx = \frac{\pi}{z\sqrt{1-\frac{1}{z^2}}}. \tag{2.33}$$

With the same procedure, using complex residue calculus, the approximation $I_m(f)$ can be expressed as a contour integral over Γ as

$$I_m(f) = \sum_{k=1}^{m} w_k f(x_k) + R_m = \frac{1}{2\pi i} \int_\Gamma f(z) r_m(z)\, dz + R_m, \tag{2.34}$$

where by substituting $w_k = \pi/m$ and $x_k = \cos(2k-1)\pi/2m$ into r_m, hence r_m is defined by

$$r_m(z) = \sum_{k=1}^{m} \frac{w_k}{z - x_k} = \frac{\pi}{n} \sum_{k=1}^{m} \frac{1}{z - \cos(\frac{(2k-1)\pi}{2m})}. \tag{2.35}$$

Then R_m is given by

$$R_m = I(f) - I_m(f) = \frac{1}{2\pi i} \int_\Gamma f(z)(\phi(z) - r_m(z))\, dz, \tag{2.36}$$

where $\phi(z)$, $r_m(z)$ are defined by (2.33) and (2.35). However, this expression for R_m can not be exactly evaluated, but tight upper bounds may reveal the convergence behaviour.

Also, from (2.36), it follows that [42, Theorem 2.48]

$$|R_m| \le \frac{l(\Gamma)}{2\pi} \max_{z \in \Gamma} |\phi(z) - r_m(z)| \cdot \max_{z \in \Gamma} |f(z)|, \tag{2.37}$$

where $l(\Gamma)$ is the length of contour Γ.

Figure 2.6 shows errors $|\phi(z) - r_m(z)|$ as contour plots in the complex plane with $m = 8$ and $m = 16$. In each case, the contours correspond to the levels

18

$1, 10^{-2}, 10^{-4}, ..., 10^{-14}$ from inner to outer circle. Thus, $|\phi(z) - r_m(z)|$ decreases as the contours move away from $[-1, 1]$. For a given value of m, (2.37) gives a upper boundary of R_m for a contour far from $[-1, 1]$, where the contour is limited to where f is analytic. From another point, the desired accuracy can be achieved only by increasing m, since for an analytic function f with a small neighbourhood of $[-1, 1]$, the bound of R_m will not be small due to the closer contour chosen.

One example of the relationship between the GCQ error bound for BER of BPSK and the number of nodes is shown in Figure 2.7. The analytic function is $f(x) = \frac{1}{2\pi} \frac{x+1}{x+1+2\bar{\gamma}}$, which has a pole at $-(1 + 2\bar{\gamma})$. Thus, the radius r of the circular contour Γ chosen should be $1 < r < (1 + 2\bar{\gamma})$ such that f is analytic in $|z| \leq r$. For $\bar{\gamma}$ in the region from $-10\,\mathrm{dB}$ to $10\,\mathrm{dB}$, the region of analyticity is $|z| < 1.2$, $|z| < 3$, $|z| < 21$, $|z| < 201$, respectively. The bound derived in [43],

$$|R_m| \leq \frac{1.05}{r^{2m-2}(2m)^{1/2}} \left(\frac{1}{r^4 - 1} \right)^{1/2} ||f||, \qquad (2.38)$$

is used for the plot where $||f||^2 = \int_0^{2\pi} |f(re^{i\phi})|^2 \, d\phi$.

Figure 2.7 reveals that at low SNR values, the classical GCQ has a slow convergence rate; i.e., for the $R_m = 10^{-15}$, it requires $m = 92$ for $\gamma = -10\,\mathrm{dB}$, $m = 15$ for $\gamma = 0\,\mathrm{dB}$, $m = 6$ for $\gamma = 10\,\mathrm{dB}$, and $m = 3$ for $\gamma = 20\,\mathrm{dB}$ to converge. Thus, the convergence rate of classical GCQ rule improves dramatically for large SNR values. However, the low convergence rate in low SNR suggests the usage of rational GCQ rule.

2.4.3 Rational GCQ

The adopted rational GCQ rule was derived by Deun, Bultheel, and Gonzalez-Vera in [40] and is briefly described in Dhungana's paper [2]. The appearance of classical and rational GCQ has the same format, except for the computation of weights w_k and nodes x_k. In the following sections, preliminaries of Chebyshev orthogonal rational functions are illustrated first, and then rational GCQ approximation rule for the weights and nodes calculation is presented.
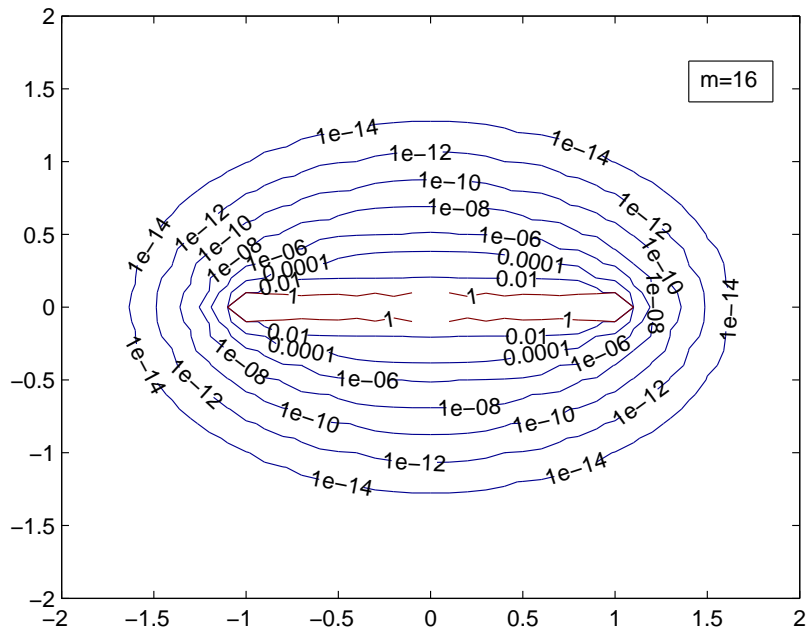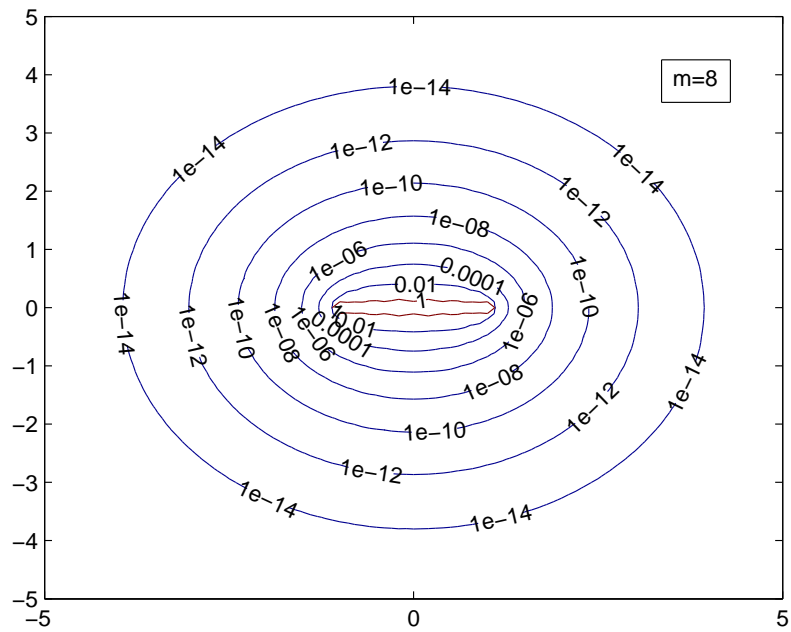
Figure 2.6: Contour plots of the error $|\phi(z) - r_m(z)|$ for the GCQ formulas with $m = 8$ and 16.
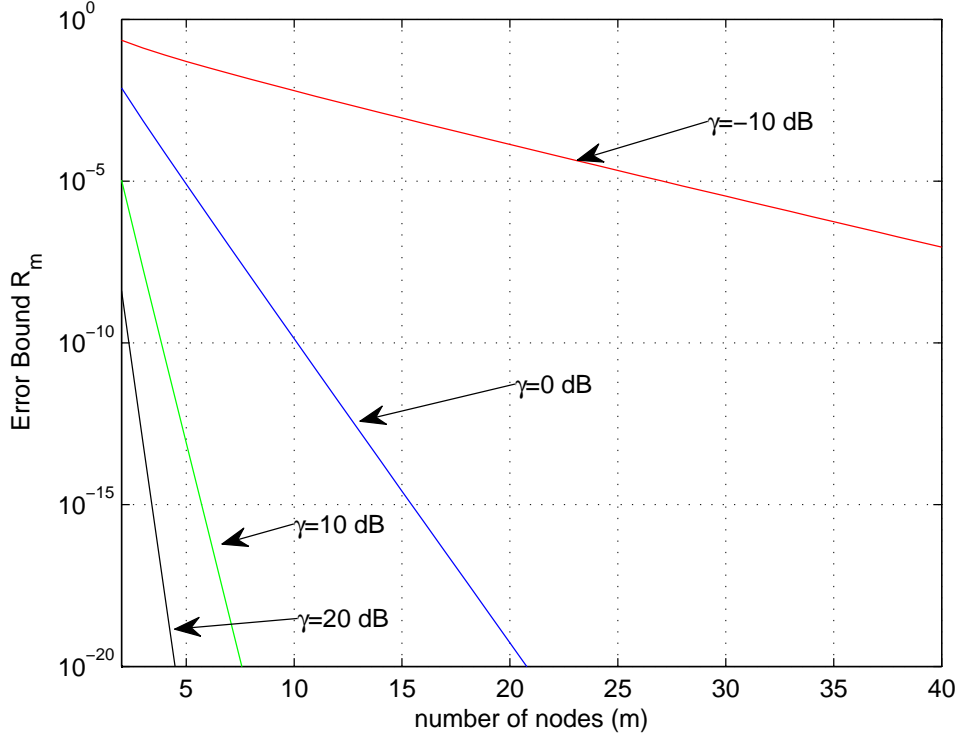
Figure 2.7: GCQ error bound for the BER of BPSK over Rayleigh fading [2]

Chebyshev orthogonal rational functions

The Chebyshev orthogonal rational function is defined as

$$Z_k(x) = \frac{b_k x^k + b_{k-1} x^{k-1} + ... + b_0 x^0}{(1 - x/\alpha_k)(1 - x/\alpha_{k-1})...(1 - x/\alpha_1))}, k = 1, 2, ... \qquad (2.39)$$

where $\{\alpha_1, \alpha_2, ...\}$ is a sequence of real poles outside $[-1, 1]$. All Z_k must be orthogonal over $W(x) = 1/\sqrt{1 - x^2}$ on $[-1, 1]$, and Z_k are called ***Chebyshev orthogonal rational functions***. In the special case of all $\alpha_k = \infty$, then (2.39) reduces to ***Chebyshev polynomials*** of degree k.

Rational GCQ rule

Through the Joukowski transformation $x = \frac{1}{2}(z + z^{-1})$, denoted as $x = J(z)$, the unit circle is mapped onto the interval $[-1, 1]$ and points outside the interval $[-1, 1]$ are mapped onto the range $|z| < 1$. With the sequence of real poles $\{\alpha_1, \alpha_2, ...\}$

21

outside this interval, we associated a sequence of $\{\beta_1, \beta_2, ...\}$ where $\beta_k = J^{-1}(\alpha_k)$ should lie in the range of $|\beta_k| < 1$.

The nodes $\{x_k\}_{k=1}^n$ in the n nodes rational GCQ rule (2.31) can be computed as $x_k = \cos(\theta_k)$ where θ_k is the only zero on $(0,\pi)$ of a real-valued function $f_n(\theta_k)$ that strictly increases over the interval $(0,\pi)$:

$$
f_n(\theta_k) = 2 \sum_{j=1}^{n-1} \arctan \frac{\sin \theta_k}{\cos \theta_k - \beta_j} + \arctan \frac{\sin \theta_k}{\cos \theta_k - \beta_n}
$$
$$
- (n-1)\theta_k - \pi/2 \, (2k-1). \tag{2.40}
$$

The corresponding weight equations w_k in (2.31) can be derived as

$$
w_k = 2\pi \, (1 + g_n(x_k))^{-1}, \quad k = 1, 2, \ldots, n, \tag{2.41}
$$

where

$$
g_n(x_k) = 2 \sum_{j=1}^{n-1} \frac{\sqrt{1 - 1/\alpha_j^2}}{1 - x/\alpha_j} + \frac{\sqrt{1 - 1/\alpha_n^2}}{1 - x/\alpha_n}. \tag{2.42}
$$

Theorem: *The above function f_n is strictly increasing for $0 \leq \theta \leq \pi$, then we have $0 \leq \theta_1 < \theta_2 < \ldots < \theta_n \leq \pi$. Furthermore, the function f_n is concave on $(0,\pi)$ if all the poles are positive, and convex if all the poles are negative. If there are both positive and negative poles, $f_n(\theta_k)$ has only one inflection point in the interval of $(0,\pi)$.*

Newton's method is introduced into this monotonic function for finding the zeros θ_k of $f_n(\theta_k)$. In our computation of interest, there are two possible choices of poles, which are all poles are either all positive or all negative. For the case where all poles are positive, as a strictly increasing concave function, the iterations of Newton's method can rapidly converge towards to the actual result if the initial guess value is less from the exact solution. With the initial guess of $\theta_0 = \theta_1 = 0$ and the linear extrapolation of $\theta_{k+1} = \theta_k + (\theta_k - \theta_{k-1})$, the zeros of f_n can be easily obtained. For the case where all poles are negative, the procedure is similar, but with the initial guess of $\theta_n = \theta_{n+1} = \pi$ and the linear extrapolation of $\theta_{k-1} = \theta_k + (\theta_k - \theta_{k+1})$, then the zeros of f_n can be obtained.

2.5   Conclusion

This chapter provided background material for digital modulation schemes and GCQ rules. ASK, PSK, QAM and FSK modulation schemes were described. Generalized integral for performance metrics analysis, such as outage, BER/SER, and capacity, was presented. Mathematical tools, such as classical and rational GCQ rules, and convergence rate, were described.

$$\sim$$

Chapter 3

GCQ rules for SER

Chapter 2 introduced several digital modulation schemes. This chapter develops an exact analysis and two Gaussian quadrature rules, named classical and rational GCQ, for the approximation analysis of digital modulation schemes.

3.1 Introduction

In this chapter, classical and rational GCQ rules are adopted for SER of several modulation schemes. Widely used multipath fading models of Rayleigh, Rician and Nakagami-m fading are considered. Numerical examples are provided to demonstrate the high accuracy of using the GCQ rules for SER.

The error performance of digital modulations over many fading channels has been extensively analyzed in the literature. Different approaches include analytically simple and tight closed-form bounds and approximations for Gaussian integral function [20–28], characteristic function method [44], asymptotic analysis approach [45], and alternative Craig's exponential integral representations for the Q-function and its corresponding Gaussian integral function [19]. Nevertheless, simple GCQ approximations are highly desirable.

The rest of this chapter is organized as follows. Rayleigh, Rician and Nakagami-m fading models are described in Section 3.2. The CEP of selected digital modulation schemes is presented in Section 3.3. The rational GCQ rule and classical GCQ rule for error probability of each digital modulation are illustrated in Section 3.4. Numerical and simulation examples are presented in Section 3.5. Finally, Section

3.6 concludes the chapter.

3.2 System Model

The basic model of wireless transmission is shown in Figure 3.1. The received signal $\tilde{r}(t)$ through the channel can be represented as

$$\tilde{r}(t) = \alpha \cdot \tilde{s}(t) + n(t), \tag{3.1}$$

where $\tilde{s}(t)$ is transmitted signal, $n(t)$ is zero-mean additive white Gaussian noise (AWGN) with power spectral density $N_0/2$, and α is the channel gain. In a non-fading channel, α is set equal to unity. In a fading channel, the distribution of α depends on the type of fading models.
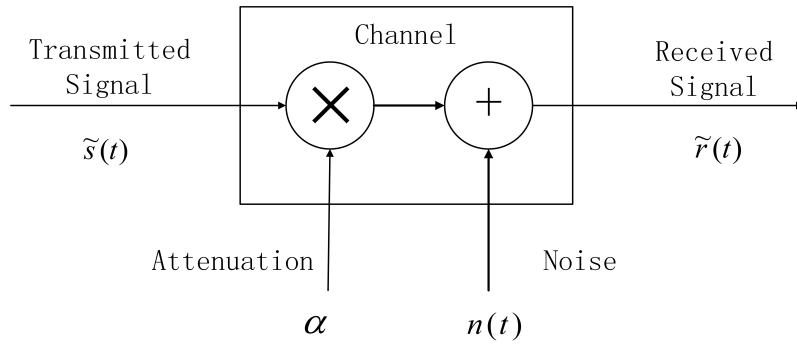
Figure 3.1: Channel Model

3.2.1 Non-fading Channels

Here, the received signal is simply given by

$$\tilde{r}(t) = \tilde{s}(t) + n(t), \tag{3.2}$$

where $\tilde{r}(t)$ is the received signal, $\tilde{s}(t)$ is the transmitted digitally modulated signal, i.e., ASK, PSK, QAM, and FSK explained in Chapter 2, and $n(t)$ is a zero-mean AWGN parameter with the power spectral density of $N_0/2$. The probability density function (PDF) of n is given by [1]

$$p(n) = (\frac{1}{\sqrt{\pi N_0}})e^{-\frac{n^2}{N_0^2}}. \tag{3.3}$$

25

3.2.2 Rayleigh Fading

Rayleigh fading is one of the commonly used multipath fading models, which describes radio links with no direct line-of-sight (LOS) [1]. When radio links are subject to Rayleigh fading, SNR per symbol $\gamma = \xi_s/N_0$ follows exponential distribution as

$$p_\gamma(\gamma) = \frac{1}{\bar{\gamma}}\exp(-\frac{\gamma}{\bar{\gamma}}), \qquad 0 \leq \gamma < \infty, \tag{3.4}$$

where $\bar{\gamma}$ is the average SNR.

The moment generating function (MGF) of γ, $\varphi_\gamma(s) = \mathbb{E}[e^{-s\gamma}]$, can be written as [1]

$$\varphi_\gamma(s) = \int_0^\infty e^{-s\gamma} p_\gamma(\gamma)\, d\gamma = \frac{1}{1 + s\bar{\gamma}}. \tag{3.5}$$

The MGF is necessary in order to use the GCQ rules.

3.2.3 Rician Fading

Rician fading characterizes channels consisting of a dominant direct LOS component and multiple random components. Thus, with Rician fading, the PDF of the instantaneous SNR per symbol is given by [1]

$$p_\gamma(\gamma) = \frac{(1+K)e^{-K}}{\bar{\gamma}}\exp[-\frac{(1+K)\gamma}{\bar{\gamma}}]I_0(2\sqrt{\frac{K(1+K)\gamma}{\bar{\gamma}}}), \; \gamma \geq 0, \tag{3.6}$$

where $0 \leq K < \infty$ is the Rician factor, and $I_0(.)$ is the zeroth-order modified Bessel function of the first kind [1, 39]. Rayleigh fading is a special case of Rician fading model when $K = 0$.

The MGF of SNR γ can be written as

$$\varphi_\gamma(s) = \frac{1+K}{1+K+s\bar{\gamma}}\exp\left(\frac{Ks\bar{\gamma}}{1+K+s\bar{\gamma}}\right). \tag{3.7}$$

3.2.4 Nakagami-m Fading

This is a versatile statistical model which can represent a variety of fading environments. When radio links are subject to Nakagami-m fading, SNR γ has the PDF,

$$p_\gamma(\gamma) = \frac{m^m \gamma^{m-1}}{\bar{\gamma}^m \Gamma(m)}\exp\left(-\frac{m\gamma}{\bar{\gamma}}\right), \quad \gamma \geq 0 \tag{3.8}$$

where m is the Nakagami-m fading parameter, which ranges from $\frac{1}{2}$ to ∞. This model reduces to Rayleigh fading when $m = 1$.

The MGF of γ can be written as

$$\varphi_\gamma(s) = \left(1 + \frac{s\bar{\gamma}}{m}\right)^{-m}. \tag{3.9}$$

3.3 Error Probability

The transmitter side of various digital modulation schemes has already been discussed in Chapter 2. In this section, the receiver of coherent detection and non-coherent detection of selected digital modulations is presented. In particular, the conditional BER/SER expressions are derived.

3.3.1 Coherent Detection of ASK

In coherent detection, the receiver reconstructs the carrier with perfect knowledge of the phase and frequency. The received signal $\tilde{r}(t)$ reconstructs the transmitted signal $\tilde{s}(t)$ with perfect knowledge of the transmitter. A matched filter and decision device provide output symbols in Figure 3.2.
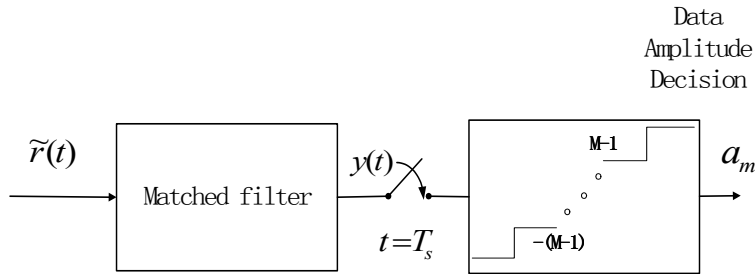

Figure 3.2: Optimum Receiver of Amplitude Shift Keying [1]

Details of acquiring minimum Euclidean distance for signalling detection have already been discussed in Chapter 2. According to geometric implementation, the Euclidean distance region of bisector for two signal points is illustrated in Figure 3.3. An error occurs if $\tilde{r}$ is in D_2 for transmitted signal $\tilde{s}_1$ sending. This error means the distance between the projection of $\tilde{r} - \tilde{s}_1$ on $\tilde{s}_2 - \tilde{s}_1$, i.e., point A, from s_1 is larger than $\frac{d_{12}}{2}$, where $d_{12} = ||\tilde{s}_2 - \tilde{s}_1||$. For the transmitted signal s_1 in AWGN

channel, the noise is $n = \tilde{r} - \tilde{s}_1$, zero-mean Gaussian noise with variance of $\frac{d_{12}^2 N_0}{2}$, and the projection of $\tilde{r} - s_1$ on $\tilde{s}_2 - \tilde{s}_1$ is equal to $\frac{n \cdot (\tilde{s}_2 - \tilde{s}_1)}{d_{12}}$. The error probability in terms of Euclidean distance is given by [1]

$$
\begin{aligned}
P_e &= \mathbb{P}[\frac{n \cdot (\tilde{s}_2 - \tilde{s}_1)}{d_{12}} > \frac{d_{12}}{2}] \\
&= \mathbb{P}[n \cdot (\tilde{s}_2 - \tilde{s}_1) > \frac{d_{12}^2}{2}] \\
&= Q\left(\frac{\frac{d_{12}^2}{2}}{d_{12}\sqrt{\frac{N_0}{2}}}\right) = Q\left(\frac{d_{12}}{\sqrt{2N_0}}\right).
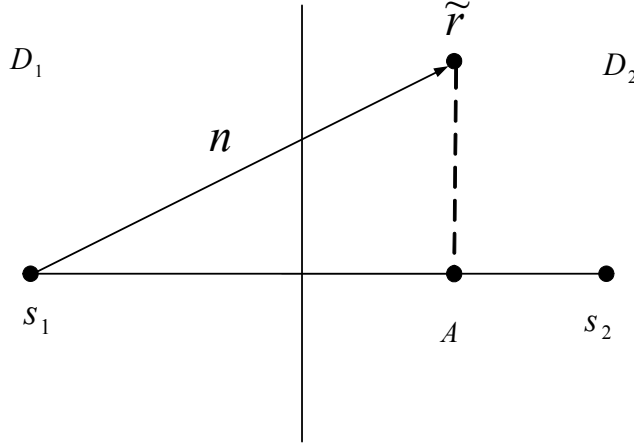\end{aligned}
\tag{3.10}
$$

Figure 3.3: Binary equiprobable signals' decision regions

Specific coherent detection of ASK modulation is presented below.

M-ary ASK

As we assuming all the signals are equiprobable, the error probability for M-ary ASK follows the procedure of bisector for two signal points. The constellation for M-ary ASK is shown in Figure 3.4 in terms the minimum distance, d_{min}, which is given (2.6) as

$$
d_{min} = \sqrt{\frac{12\log_2 M}{M^2 - 1}} \xi_b.
\tag{3.11}
$$

The constellation points are located at $\{\pm\frac{1}{2}d_{min}, \pm\frac{3}{2}d_{min}, \ldots, \pm\frac{M-1}{2}d_{min}\}$.

The two types of points in the M-ary ASK constellation are the $M - 2$ inner points and the 2 outer points in the constellation. Each inner point has two detection
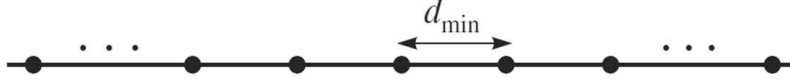
28

Figure 3.4: The ASK constellation [1]

regions, and the outer points have only one detection region. According to (3.10), the error probabilities for the inner points and outer points are given as [1]

$$P_{ei} = \mathbb{P}[|n| > \frac{1}{2}d_{min}] = 2Q\left(\frac{d_{min}}{\sqrt{2N_0}}\right), \qquad (3.12)$$

$$P_{eo} = \mathbb{P}[n > \frac{1}{2}d_{min}] = Q\left(\frac{d_{min}}{\sqrt{2N_0}}\right). \qquad (3.13)$$

The total symbol error probabilities are given as [1]

$$\begin{aligned} P_e &= \frac{1}{M}\sum_{m=1}^{M}\mathbb{P}[error|a_m \text{ sent}] \\ &= \frac{1}{M}[2(M-2)P_{ei} + 2 \cdot P_{eo}] \\ &= \frac{2(M-1)}{M}Q\left(\frac{d_{min}}{\sqrt{2N_0}}\right). \end{aligned} \qquad (3.14)$$

Substituting the right-hand side of (3.11) for d_{min} and using the instantaneous SNR per bit $\gamma_b = \xi_b/N_0$ yields [1]

$$P_e = \frac{2(M-1)}{M}Q\left(\sqrt{\frac{6}{M^2-1}\gamma_b\log_2 M}\right). \qquad (3.15)$$

One example of ASK modulation is BASK ($M = 2$, $\gamma = \gamma_b$). Therefore, the probability of error is given as

$$P_e = Q(\sqrt{2\gamma}). \qquad (3.16)$$

3.3.2 Coherent Detection of PSK

With the same assumption of coherent detection, the received signal at receiver side is $\tilde{r}(t) = \tilde{s}(t) + n(t)$. In the PSK modulation, $\tilde{s}$ refers to $e^{j\theta_m}g(t)$, where m is in the range of $1 \leq m \leq M$ and $g(t)$ is same for each signal which can be omitted. One

familiar PSK modulation is BPSK, which corresponds to $M = 2$. Therefore, the values of θ_m can be chosen as 0 and π, which correspond to $e^{j \cdot 0} = 1$ and $e^{j \cdot \pi} = -1$. The receiver is depicted in Figure 3.5.

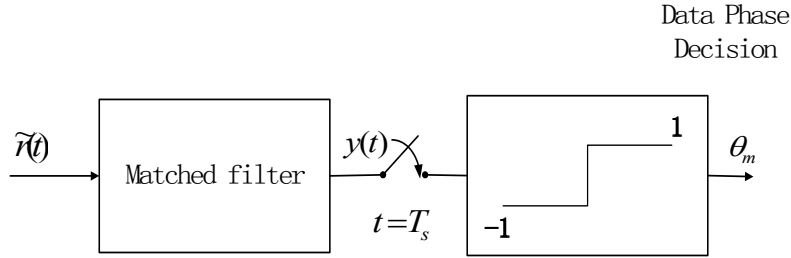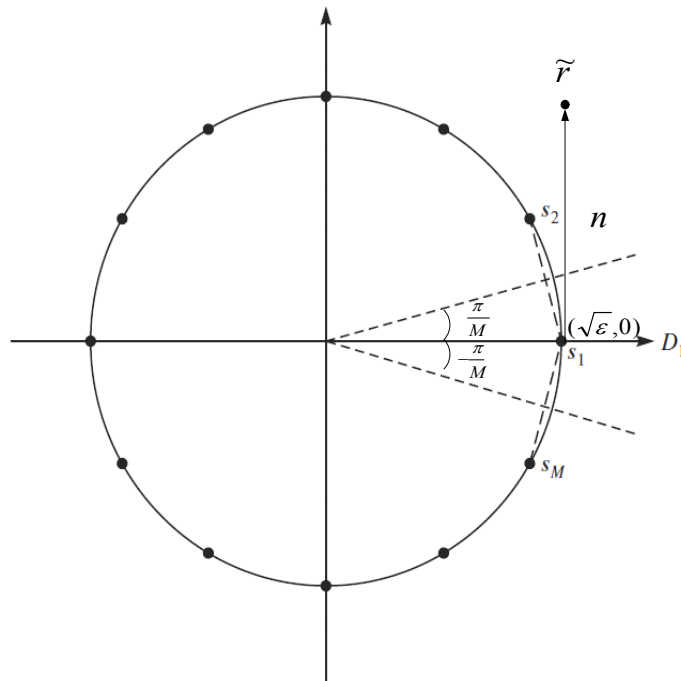Figure 3.5: Optimum Receiver of Phase Shift Keying [1]

Figure 3.6: PSK signalling constellation

According to (2.9), PSK is two dimensional for each transmitted signal. In Figure 3.6, the PSK constellation is shown along with the decision region D_1. For the transmitted signal $s_1 = (\sqrt{\xi}, 0)$, the received vector $\tilde{r}$ is given by

$$r = (r_1, r_2) = (\sqrt{\xi} + n_1, n_2) \tag{3.17}$$

where n_1, n_2 are noise of independent Gaussian random variables with variance $\delta^2 = \frac{1}{2}N_0$, and means are both 0. The joint PDF of (n_1, n_2) is given by [1]

$$p(n_1, n_2) = \frac{1}{\pi N_0}e^{-\frac{n_1^2+n_2^2}{N_0}}. \tag{3.18}$$

By using the transformation of polar coordinates, the new variables are given by $V = \sqrt{n_1^2 + n_2^2}$ and $\Theta = \arctan\frac{n_2}{n_1}$. Then, the joint PDF of V and Θ is given as [1]

$$p_{V,\Theta}(v, \theta) = \frac{v}{\pi N_0}e^{-\frac{v^2}{N_0}}. \tag{3.19}$$

The decision region is partitioned into M regions denoted by $D_1, D_2, ..., D_M$ such that if $\tilde{r} \in D_m$, then $\hat{\theta}_m = \theta_m$. The region D_m, $1 \leq m \leq M$, is called the decision region for transmitted signal a_m. In Figure 3.6, the decision region D_1 is described as $D_1 = \{\theta : -\pi/M < \theta < \pi/M\}$.

Specific coherent detection of PSK modulation is presented below.

M-ary PSK

As we discussed above, we have the transformation of the PSK signalling constellations in the polar coordinates system. The M-ary PSK follows the same procedure. The constellation for M-ary PSK is shown in Figure 3.7. Only point s_1 and its decision region are shown here. The shaded area, which can extend to infinity, shows the error region when s_1 is transmitted.

One conventional transformation is to let the new polar coordinates system's origin be at $\sqrt{\xi}$, which is shown in Figure 3.8. Therefore, the error probability is $P[(n_1, n_2) \in \text{shaded area}]$. The new polar coordinates system is given as [1]

$$r = \sqrt{n_1^2 + n_2^2}, \tag{3.20}$$

$$\varsigma = \arctan\frac{n_2}{n_1}, \tag{3.21}$$

where n_1 and n_2 are independent Gaussian random variables with zero means and variance $\delta^2 = \frac{1}{2}N_0$. The length of R is a function in terms of θ and is given as [1]

$$R(\theta) = \sqrt{\xi}\sin\frac{\pi}{M} \cdot \frac{1}{\sin\theta}. \tag{3.22}$$
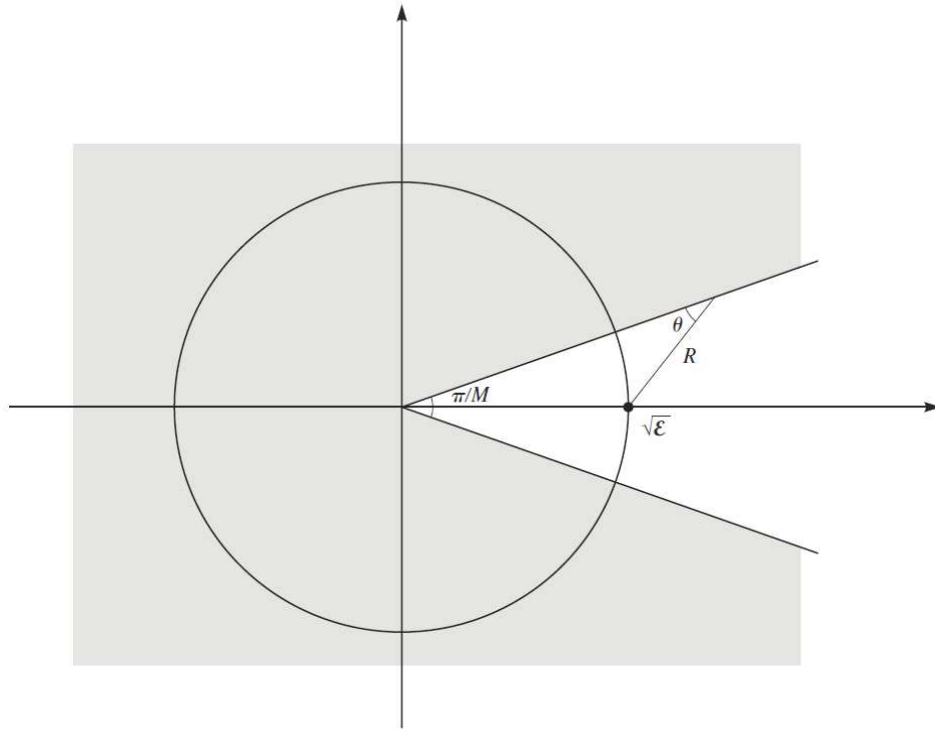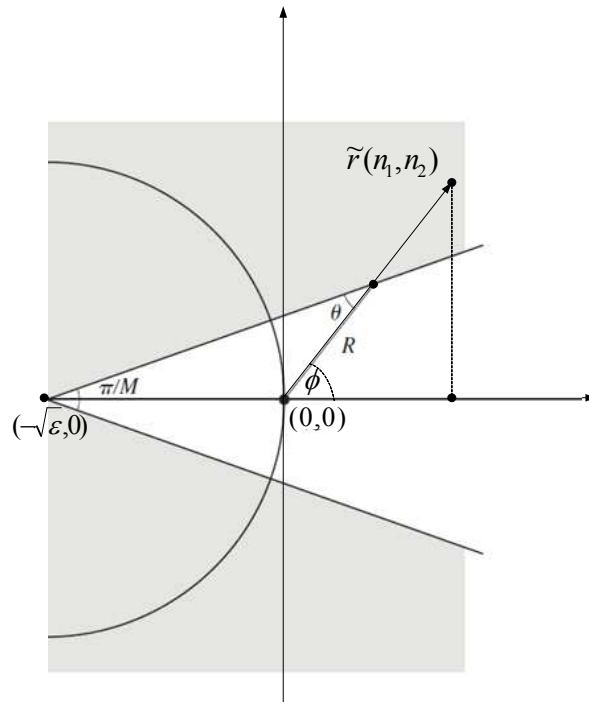
Figure 3.7: Signalling constellation of MPSK system [1]

Figure 3.8: Polar coordinates system for MPSK constellation

Therefore, the error probability is given as [1]

$$P_e = \int_{\frac{\pi}{M}}^{2\pi - \frac{\pi}{M}} d\varsigma \int_R^\infty \frac{r}{\pi N_0} \exp\left(-\frac{r}{N_0}\right) dr$$

$$= 2 \int_{\frac{\pi}{M}}^{\pi} d\varsigma \int_R^\infty \exp\left(-\frac{\xi \sin\frac{\pi}{M}}{N_0 \sin^2(\phi - \pi/M)}\right) dr$$

$$= \frac{1}{\pi} \int_0^{\frac{(M-1)\pi}{M}} \exp\left(-\frac{\xi}{N_0} \frac{\sin^2\frac{\pi}{M}}{\sin^2\theta}\right) d\theta. \tag{3.23}$$

Substituting instantaneous SNR per bit $\gamma_b = \xi_b/N_0$ and using the relationship between instantaneous SNR per bit and SNR per symbol $\gamma = \gamma_b\log_2 M$ yields

$$P_e = \frac{1}{\pi} \int_0^{\frac{(M-1)\pi}{M}} \exp(-\frac{g_{psk}\log_2 M\gamma_b}{\sin^2\theta}) d\theta, \quad \text{where } g_{psk} = \sin^2\frac{\pi}{M}. \tag{3.24}$$

The most commonly used PSK modulation scheme is BPSK, where $M = 2$. Therefore, the probability of error is given as

$$P_e = \frac{1}{\pi} \int_0^{\frac{\pi}{2}} \exp\left(-\frac{\gamma}{\sin^2\theta}\right) d\theta = 2Q(\sqrt{2\gamma}), \tag{3.25}$$

where in the case of BPSK, γ and γ_b are equivalent.

3.3.3 Coherent Detection of squared QAM

Coherent detection of QAM follows the same procedure as that for ASK. The received signal $\tilde{r}(t) = \tilde{s}(t) + n(t)$, where $\tilde{s}(t)$ refers to $\text{Re}[(a_{mi} + ja_{mq})g(t)e^{j2\pi f_c t}]$, where $g(t)e^{j2\pi f_c t}$ is same and is omitted here. The receiver is depicted in Figure 3.9.

Squared M-ary QAM

For the squared M-ary QAM, the signal constellation is shown as Figure 2.4. Since the in-phase term a_{mi} and quadrature-phase term a_{mq} both take the equiprobable values of their information amplitudes, M-ary QAM can be considered as two $\sqrt{M}$-ary ASK constellations in the in-phase and quadrature directions. By using the same procedure of bisector for two signal points, the constellation can be considered in terms of d_{min} as well as M-ary ASK modulation, where d_{min} is given (2.19) as

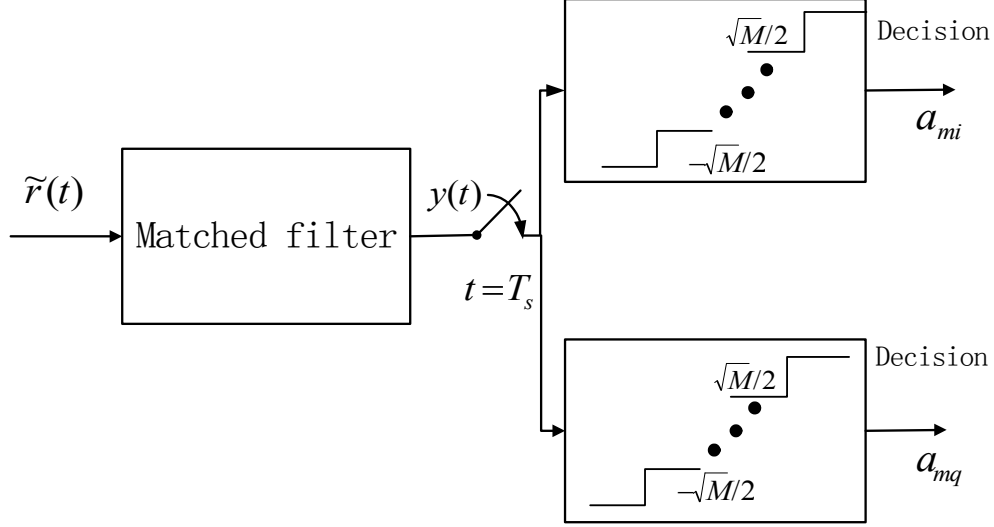$$d_{min} = \sqrt{\frac{6\log_2 M}{M - 1}\xi_b}. \tag{3.26}$$

Figure 3.9: Optimum Receiver of Quadrature Amplitude Modulation [1]

The probability of the correct detection for M-ary QAM is the product of correct decision probabilities for constituent ASK modulation; i.e., [1]

$$P_{c,M-\text{QAM}} = P^2_{c,\sqrt{M}-\text{ASK}} = (1 - P_{e,\sqrt{M}-\text{ASK}})^2. \tag{3.27}$$

Therefore, the error probability is given by [1]

$$P_{e,M-\text{QAM}} = 1 - P_{c,M-\text{QAM}} = 2P_{e,\sqrt{M}-\text{ASK}} - P^2_{e,\sqrt{M}-\text{ASK}}. \tag{3.28}$$

According to (3.14) and (3.26), the probability of error is simplified to [1]

$$P_{e,M-\text{QAM}} = 4(\frac{\sqrt{M}-1}{\sqrt{M}})Q\left(\sqrt{\frac{3}{M-1}\gamma_b\log_2 M}\right)$$
$$- 4(\frac{\sqrt{M}-1}{\sqrt{M}})^2 Q^2\left(\sqrt{\frac{3}{M-1}\gamma_b\log_2 M}\right). \tag{3.29}$$

The most commonly used QAM modulation is 4-QAM, which is $M = 4$. For 4-QAM,

$$P_e = 2Q(\sqrt{2\gamma}) - Q^2(\sqrt{2\gamma}). \tag{3.30}$$

3.3.4   Coherent Detection of FSK

The received signal for coherent FSK is $\tilde{r}(t) = \tilde{s}(t) + n(t)$. The decision about the transmitted signal is based on the largest frequency. The receiver is depicted in Figure 3.10.
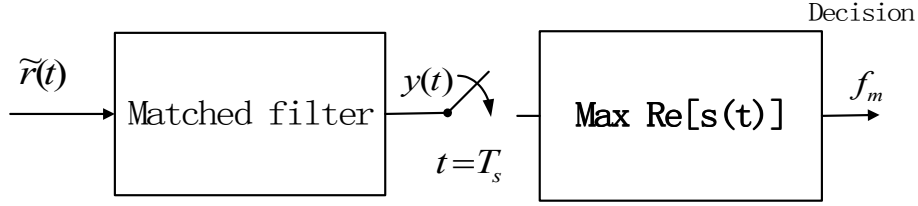
Figure 3.10: Optimum Receiver of Frequency Shift Keying [1]

In FSK, $\tilde{s}(t)$ refers to $\mathrm{Re}[e^{j2\pi f_m t}\sqrt{2\xi_g/T}e^{j2\pi f_c t}]$, where m is in the rage of $1 \leq m \leq M$, and $\sqrt{2\xi_g/T}e^{j2\pi f_c t}$ is same for each signal and is omitted here for simplification.

BFSK

One common version of FSK is BFSK, which corresponds to $M = 2$. Therefore, the frequencies of f_m are equal to f_1 and f_2, respectively. Since we assume all transmitted signals are equiprobale, the error probability for BFSK follows the procedure of bisector for two signal points. The error probability of BFSK can be expressed in terms of d_{min}, which is given (2.24) as

$$d_{min} = \sqrt{2\mathrm{log}_2 M \cdot \xi_b}. \tag{3.31}$$

Therefore, the error probability of BFSK can be obtained by substituting d_{min} from (3.31) into the bisector determination described in (3.10) in the form of

$$P_e = Q(\frac{\sqrt{2\xi_b}}{\sqrt{2N_0}}) = Q(\sqrt{\gamma}). \tag{3.32}$$

3.3.5 Noncoherent Detection of M-ary Differential PSK

The noncoherent receiver is not perfectly synchronized with the transmitter. Thus, the received signal at receiver side is $\tilde{r}(t) = \tilde{s}(t - t_d) + n(t)$, where t_d represents a timing error. In such a case, differential PSK may be used.

Differential PSK (DPSK) is also one kind of phase modulation that conveys or modifies the phase of the signal waves. Compared to the ordinary PSK modulation explained in Section 2.1.2, the DPSK modulation does not need a constant reference

35

carrier and can operate with respect to itself; i.e., if $\Delta\theta_m$ is the information phase to be transmitted in the mth transmission interval, the transmitter would first modulate

$$\theta_m = \theta_{m-1} + \Delta\theta_m, \quad \text{modulo} \quad 2\pi, \tag{3.33}$$

and then modulate θ_m on the carrier. At the receiver side, successive decisions on θ_m and θ_{m-1} will be made depending on $\Delta\theta_m$. In Figure 3.11, the receiver side of two adjacent phase decisions for a differentially encoded Quadrature PSK system is illustrated.
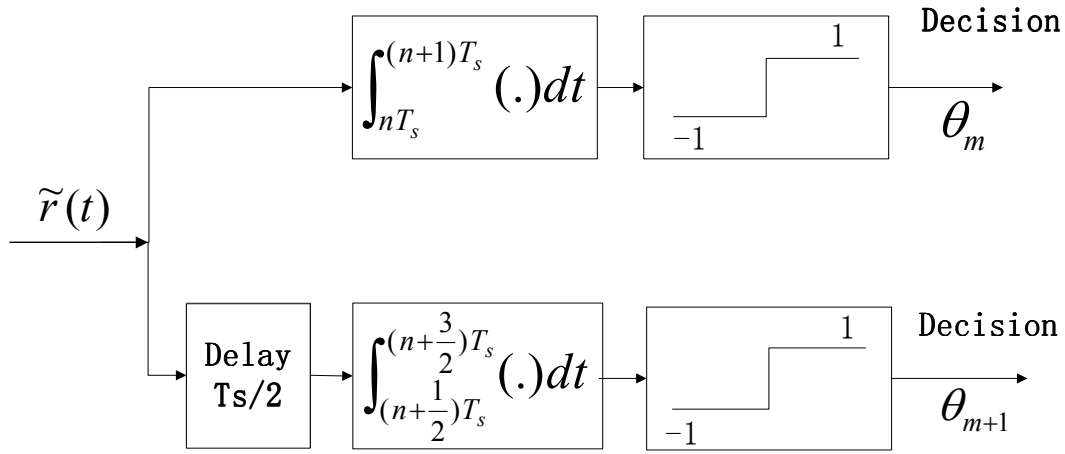

Figure 3.11: Optimum Receiver of Differential Phase Shift Keying Modulation [1]

In this modulation technique, the demodulation part determines the changes in the phase of the received signal rather than the phase of a reference carrier signal. DPSK is a simpler modulation technique than ordinary PSK modulation since DPSK does not require a coherent reference at the receiver (this technique is referred to as *noncoherent detection*) and thus it can be noncoherently demodulated. However, DPSK will produce more erroneous demodulation than the ordinary PSK's demodulation.

The error probability of M-ary DPSK is given by [46]

$$P_e = \frac{\sin\frac{\pi}{M}}{\pi} \int_0^{\frac{\pi}{2}} \frac{\exp[-\log_2 M\gamma(1 - \cos(\frac{\pi}{M}\cos\theta))]}{1 - \cos\frac{\pi}{M}\cos\theta} \, d\theta \tag{3.34}$$

$\pi/4$-Differential QPSK

The modulation technique of $\pi/4$-DQPSK is based on the QPSK modulation. The ordinary QPSK modulation is a special case of M-ary PSK; i.e., $M = 4$, and the phase set, θ_m, is chosen from $0, \pi/2, \pi, 3\pi/2$ to represent the information phases. By converting with the initial transmitted phase $\pi/4$, the ordinary QPSK is converted to the conventional form of Differential QPSK (DQPSK) modulation, in which the θ_m is range over the set $\pi/4, 3\pi/4, 5\pi/4, 7\pi/4$.

In the noncoherent detection of $\pi/4$-DQPSK, the receiver side's phase decisions $\Delta\theta_m$ are based on

$$\Delta\theta_m = \frac{(2k-1)\pi}{4}, \quad k = 1, 2, 3, 4; \tag{3.35}$$

i.e., the phase angles are $\pi/4, 3\pi/4, 5\pi/4, 7\pi/4$, in each symbol duration T_s. The error probability of $\pi/4$-DQPSK is given by [47]

$$P_e = \frac{1}{2\pi} \int_0^\pi \exp\left(\frac{\gamma(b^2 - a^2)^2}{2(a^2 + b^2) - 4ab\cos\theta}\right) d\theta, \tag{3.36}$$

where $a = \sqrt{(1 - \sqrt{1 - |\rho|^2}/2)}$, $b = \sqrt{(1 + \sqrt{1 - |\rho|^2}/2)}$, and $0 \leq |\rho| \leq 1$ is the magnitude of the cross-correlation coefficient between the two signals.

3.4 Application of GCQ rules

In Section 3.3, SER expressions for selected digital modulation schemes were given. These must be averaged over the distribution of the SNR in fading channel. For our purpose, GCQ rules are introduced for calculating the CEP.

3.4.1 Error Performance of Coherent ASK

The conditional symbol error probability for coherent M-ary ASK can be expressed in the form of

$$P_s(\epsilon|\gamma_b) = \frac{2(M-1)}{M} Q\left(\sqrt{\frac{6}{M^2 - 1}\gamma_b\log_2 M}\right). \tag{3.37}$$

By using the transformation of Craig's formula in (2.27), the CEP is given as

$$P_s(\epsilon|\gamma_b) = \frac{2(M-1)}{M\pi} \int_0^{\pi/2} \exp\left(-\frac{3\gamma_b\log_2 M}{(M^2 - 1)\sin^2\theta}\right) d\theta. \tag{3.38}$$

By changing the variables $\cos(2\theta) = x$, the CEP of (3.38) can be transformed into the desired form of GCQ rule as

$$P_s(\epsilon|\gamma_b) = \frac{M-1}{M\pi} \int_{-1}^{+1} \frac{\exp\left(\frac{\frac{6}{M^2-1}\log_2 M\gamma_b}{x-1}\right)}{\sqrt{1-x^2}} \, dx. \tag{3.39}$$

For BASK, 4-ASK, 8-ASK, which is $M = 2$, $M = 4$, $M = 8$ respectively, the CEP in the desired form of GCQ rule is given as

$$P_b(\epsilon|\gamma_b) = \frac{1}{2\pi} \int_{-1}^{+1} \frac{\exp\left(\frac{2\gamma_b}{x-1}\right)}{\sqrt{1-x^2}} \, dx, \quad \text{BASK}, \tag{3.40}$$

$$P_s(\epsilon|\gamma_b) = \frac{3}{4\pi} \int_{-1}^{+1} \frac{\exp\left(\frac{\frac{4}{5}\gamma_b}{x-1}\right)}{\sqrt{1-x^2}} \, dx, \quad 4-\text{ASK}, \tag{3.41}$$

$$P_s(\epsilon|\gamma_b) = \frac{7}{8\pi} \int_{-1}^{+1} \frac{\exp\left(\frac{\frac{2}{7}\gamma_b}{x-1}\right)}{\sqrt{1-x^2}} \, dx, \quad 8-\text{ASK}. \tag{3.42}$$

where in BASK, there is only conditional bit error probability instead of the conditional symbol error probability.

3.4.2   Error Performance of Coherent PSK

The conditional symbol error probability for coherent M-ary PSK can be expressed in the form of

$$P_s(\epsilon|\gamma_b) = \frac{1}{\pi} \int_0^{\frac{(M-1)\pi}{M}} \exp\left(-\frac{g_{psk}\log_2 M\gamma_b}{\sin^2\theta}\right) d\theta, \quad \text{where } g_{psk} = \sin^2\frac{\pi}{M}. \tag{3.43}$$

Through the variable substitution of $x = \cos(M\theta/(M-1))$, the desired form of GCQ rule can be expressed as

$$P_s(\epsilon|\gamma_b) = \frac{M-1}{M\pi} \int_{-1}^{+1} \frac{\exp\left(\frac{g_{psk}\log_2 M\gamma_b}{\sin^2(\frac{M-1}{M}\cos^{-1}(x))}\right)}{\sqrt{1-x^2}} \, dx, \quad \text{where } g_{psk} = \sin^2\frac{\pi}{M}. \tag{3.44}$$

One immediate observation can be found is that the upper limit of (3.43) is $(M-1)\pi/M$, i.e., an arbitrary number. Through the variable substitution of $x = \cos(M\theta/(M-1))$, any integration with an arbitrary upper limit can be expressed in the form of GCQ rule.

For BPSK, 4-PSK, 8-PSK, which is $M = 2$, $M = 4$, and $M = 8$ respectively, the CEP in desired form of GCQ rule is given as

$$P_b(\epsilon|\gamma_b) = \frac{1}{2\pi} \int_{-1}^{+1} \frac{\exp\left(\frac{2\gamma_b}{x-1}\right)}{\sqrt{1-x^2}} \, dx, \quad \text{BPSK}, \tag{3.45}$$

$$P_s(\epsilon|\gamma_b) = \frac{3}{4\pi} \int_{-1}^{+1} \frac{\exp\left(\frac{\gamma_b}{\sin^2(\frac{3}{4}\cos^{-1}(x))}\right)}{\sqrt{1-x^2}} \, dx, \quad 4-\text{PSK}, \tag{3.46}$$

$$P_s(\epsilon|\gamma_b) = \frac{7}{8\pi} \int_{-1}^{+1} \frac{\exp\left(\frac{3\sin^2\frac{\pi}{8}\gamma_b}{\sin^2(\frac{7}{8}\cos^{-1}(x))}\right)}{\sqrt{1-x^2}} \, dx, \quad 8-\text{PSK}, \tag{3.47}$$

where in BPSK, there is only conditional bit error probability instead of the conditional symbol error probability.

3.4.3 Error Performance of Coherent QAM

The conditional symbol error probability for coherent squared M-ary QAM can be expressed in the form of

$$P_s(\epsilon|\gamma_b) = 4\left(\frac{\sqrt{M}-1}{\sqrt{M}}\right) Q\left(\sqrt{\frac{3}{M-1}\gamma_b\log_2 M}\right)$$

$$- 4\left(\frac{\sqrt{M}-1}{\sqrt{M}}\right)^2 Q^2\left(\sqrt{\frac{3}{M-1}\gamma_b\log_2 M}\right). \tag{3.48}$$

Following the same procedure as that in the ASK modulation, by using the transformation of Craig's formula in (2.27) and (2.28), the CEP is given as

$$P_s(\epsilon|\gamma_b) = \frac{4}{\pi}\left(\frac{\sqrt{M}-1}{\sqrt{M}}\right) \int_0^{\frac{\pi}{2}} \exp\left(-\frac{\frac{3}{M-1}\log_2 M\gamma_b}{2\sin^2\theta}\right) d\theta$$

$$- \frac{4}{\pi}\left(\frac{\sqrt{M}-1}{\sqrt{M}}\right)^2 \int_0^{\frac{\pi}{4}} \exp\left(-\frac{\frac{3}{M-1}\log_2 M\gamma_b}{2\sin^2\theta}\right) d\theta \tag{3.49}$$

where the first term in (3.49) can be achieved as the desired form of GCQ rule following the ASK's substitution. By using the variable substitution $\cos(4\theta) = x$ for the second term, the desired form of GCQ rule for the CEP is thus given as

$$P_s(\epsilon|\gamma_b) = \frac{2}{\pi}\left(\frac{\sqrt{M}-1}{\sqrt{M}}\right) \int_{-1}^{+1} \frac{\exp\left(\frac{3\log_2 M\gamma_b}{(M-1)(x-1)}\right)}{\sqrt{1-x^2}} \, dx$$

$$- \frac{1}{\pi}\left(\frac{\sqrt{M}-1}{\sqrt{M}}\right)^2 \int_{-1}^{+1} \frac{\exp\left(\frac{3\log_2 M\gamma_b}{2(M-1)\sin^2(\frac{1}{4}\cos^{-1}x)}\right)}{\sqrt{1-x^2}} \, dx. \tag{3.50}$$

39

For 4-QAM, 16-QAM, and 64-QAM, which is $M = 4$, $M = 16$, and $M = 64$, respectively, the desired form of CEP is given as

$$P_s(\epsilon|\gamma_b) = \frac{1}{2\pi} \int_{-1}^{+1} \frac{\exp\left(\frac{2\gamma_b}{x-1}\right)}{\sqrt{1-x^2}} \, dx$$

$$- \frac{1}{4\pi} \int_{-1}^{+1} \frac{\exp\left(\frac{\gamma_b}{\sin^2\left(\frac{1}{4}\cos^{-1}x\right)}\right)}{\sqrt{1-x^2}} \, dx, \quad 4-\text{QAM}, \tag{3.51}$$

$$P_s(\epsilon|\gamma_b) = \frac{3}{2\pi} \int_{-1}^{+1} \frac{\exp\left(\frac{4\gamma_b}{5(x-1)}\right)}{\sqrt{1-x^2}} \, dx$$

$$- \frac{9}{16\pi} \int_{-1}^{+1} \frac{\exp\left(\frac{2\gamma_b}{5\sin^2\left(\frac{1}{4}\cos^{-1}x\right)}\right)}{\sqrt{1-x^2}} \, dx, \quad 16-\text{QAM}, \tag{3.52}$$

$$P_s(\epsilon|\gamma_b) = \frac{7}{4\pi} \int_{-1}^{+1} \frac{\exp\left(\frac{2\gamma_b}{7(x-1)}\right)}{\sqrt{1-x^2}} \, dx$$

$$- \frac{49}{64\pi} \int_{-1}^{+1} \frac{\exp\left(\frac{\gamma_b}{7\sin^2\left(\frac{1}{4}\cos^{-1}x\right)}\right)}{\sqrt{1-x^2}} \, dx, \quad 64-\text{QAM}. \tag{3.53}$$

3.4.4 Error Performance of Coherent FSK

The CEP for coherent BFSK can be expressed in the form of

$$P_b(\epsilon|\gamma_b) = Q(\sqrt{\gamma_b}). \tag{3.54}$$

By following the same procedures as that for ASK, and using the variable substitution of $\cos(2\theta) = x$, the desired form of CEP can be expressed as

$$P_b(\epsilon|\gamma_b) = \frac{1}{2\pi} \int_{-1}^{+1} \frac{\exp\left(\frac{\gamma_b}{x-1}\right)}{\sqrt{1-x^2}} \, dx. \tag{3.55}$$

3.4.5 Error Performance of Nocoherent modulation

The CEP for noncoherent M-ary DPSK is given by [46]

$$P_s(\epsilon|\gamma_b) = \frac{\sin\frac{\pi}{M}}{\pi} \int_0^{\frac{\pi}{2}} \frac{\exp[-\log_2 M\gamma(1 - \cos(\frac{\pi}{M})\cos\theta)]}{1 - \cos\frac{\pi}{M}\cos\theta} \, d\theta. \tag{3.56}$$

By changing of the variable, $x = \cos(2\theta)$, the desired form of CEP is acquired as

$$P_s(\epsilon|\gamma_b) = \frac{\sin\frac{\pi}{M}}{2\pi} \int_{-1}^{+1} \frac{\frac{\exp[-\gamma_b\log_2 M(1-\cos\frac{\pi}{M}\cos(\frac{1}{2}\cos^{-1}x))]}{1-\cos\frac{\pi}{M}(\cos(\frac{1}{2}\cos^{-1}x))}}{\sqrt{1-x^2}} \, dx. \tag{3.57}$$

40

For noncoherent QDPSK, which is $M = 4$, the CEP in the desired form of GCQ rule is given as

$$P_s(\epsilon|\gamma_b) = \frac{\sin\frac{\pi}{4}}{2\pi} \int_{-1}^{+1} \frac{\frac{\exp[-2\gamma_b(1-\cos\frac{\pi}{4}\cos(\frac{1}{2}\cos^{-1}x))]}{1-\cos\frac{\pi}{4}(\cos(\frac{1}{2}\cos^{-1}x))}}{\sqrt{1-x^2}} \, dx. \qquad (3.58)$$

The CEP for noncoherent detection of equal energy, $\pi/4$ DQPSK, is given by [47]

$$P_s(\epsilon|\gamma_b) = \frac{1}{2\pi} \int_0^\pi \exp\left(-\frac{2\gamma_b}{2-\sqrt{2}\cos\theta}\right) d\theta. \qquad (3.59)$$

By using the variable substitution of $\cos\theta = x$, the desired form of GCQ rule can be expressed as

$$P_s(\epsilon|\gamma_b) = \frac{1}{2\pi} \int_{-1}^{+1} \frac{\exp\left(\frac{-2\gamma_b}{2-\sqrt{2}x}\right)}{\sqrt{1-x^2}} \, dx. \qquad (3.60)$$

The conditional BERs/SERs of several digital modulation schemes are given in Table 3.1. To author's best knowledge, Table 3.1 has tabulated every digital modulation scheme which can adopt the GCQ rule.

Furthermore, one recognition can be acquired immediately from Table 3.1, that these expressions can be classified into two general forms

1. the simple-angle limits Gaussian Q-function, i.e., $Q(\cdot)$, which has the Craig's transformation with limits $[0, \frac{\pi}{2}]$, and

2. the multi-angle limits Gaussian integral function, i.e., the CEP of M-ary PSK, which has the limits $[0, \frac{(M-1)\pi}{M}]$.

Moreover, the simple-angle limits Gaussian Q-function can be considered as a special case of the multi-angle limits Gaussian integral function, which can be obtained through modifying the upper limits to the corresponding single angle.

The average BER/SER over the fading channels can be derived by integrating the CEP over the PDF of SNR, which can be expressed as

$$\bar{P} = \int_0^\infty P(\epsilon|\gamma)p_\gamma d\gamma = \int_{-1}^{+1} \frac{\zeta_\gamma(x)}{\sqrt{1-x^2}} \, dx, \qquad (3.61)$$

where $\zeta_\gamma(x)$ is selected and calculated with respect to the corresponding digital modulation scheme in Table 3.1.

Table 3.1: Common Digital Modulation Scheme using Gauss Chebyshev Quadrature

Coherent Modulation			
Modulation Type	Modulation Name	Conditional Error Probability $P(\epsilon\mid\gamma_b)$	Gauss Chebyshev Quadrature Format $P(\epsilon\mid\gamma_b)$
ASK	BASK	$P_b = Q(\sqrt{2\gamma_b})$	$P_b = \frac{1}{2\pi}\int_{-1}^{+1}\frac{\exp(\frac{2\gamma_b}{x-1})}{\sqrt{1-x^2}}\,dx$
	MASK	$P_s = 2(\frac{M-1}{M})$ $\cdot Q(\sqrt{\frac{6}{M^2-1}\gamma_b\log(M)})$	$P_s = \frac{M-1}{M\pi}$ $\cdot\int_{-1}^{+1}\frac{\exp\left(\frac{\frac{6}{M^2-1}\log(M)\gamma_b}{x-1}\right)}{\sqrt{1-x^2}}\,dx$
PSK	BPSK	$P_b = Q(\sqrt{2\gamma_b})$	$P_b = \frac{1}{2\pi}\int_{-1}^{+1}\frac{\exp(\frac{2\gamma_b}{x-1})}{\sqrt{1-x^2}}\,dx$
	MPSK	$P_s = \frac{1}{\pi}$ $\cdot\int_0^{\frac{(M-1)\pi}{M}}\exp(-\frac{g_{psk}\log(M)\gamma_b}{\sin^2(\theta)})\,d\theta$ where $g_{psk}=\sin^2\frac{\pi}{M}$	$P_s = \frac{M-1}{M\pi}$ $\cdot\int_{-1}^{+1}\frac{\exp(-\frac{g_{psk}\log(M)\gamma_b}{\sin^2(\frac{M-1}{M}\cos^{-1}(x))})}{\sqrt{1-x^2}}\,dx$ where $g_{psk}=\sin^2\frac{\pi}{M}$
QAM	4-QAM	$P_s = 2Q(\sqrt{2\gamma_b})$ $-Q^2(\sqrt{2\gamma_b})$	$P_s = \frac{1}{\pi}\int_{-1}^{+1}\frac{\exp(\frac{2\gamma_b}{x-1})}{\sqrt{1-x^2}}\,dx$ $-\frac{1}{4\pi}\int_{-1}^{+1}\frac{\exp(\frac{2\gamma_b}{2\sin^2(\frac{1}{4}\cos^{-1}(x))})}{\sqrt{1-x^2}}\,dx$
	Sqrared M-QAM	$P_s = 4(\frac{\sqrt{M}-1}{\sqrt{M}})$ $\cdot Q(\sqrt{\frac{3}{M-1}\gamma_b\log(M)})$ $-4(\frac{\sqrt{M}-1}{\sqrt{M}})^2$ $\cdot Q^2(\sqrt{\frac{3}{M-1}\gamma_b\log(M)})$	$P_s = \frac{2}{\pi}(\frac{\sqrt{M}-1}{\sqrt{M}})$ $\cdot\int_{-1}^{+1}\frac{\exp(\frac{3\gamma_b\log(M)}{(M-1)(x-1)})}{\sqrt{1-x^2}}\,dx$ $-\frac{1}{\pi}(\frac{\sqrt{M}-1}{\sqrt{M}})^2$ $\cdot\int_{-1}^{+1}\frac{\exp(\frac{3\gamma_b\log(M)}{2(M-1)\sin^2(\cos^{-1}(x))})}{\sqrt{1-x^2}}\,dx$
FSK	BFSK	$P_b = Q(\sqrt{\gamma_b})$	$P_b = \frac{1}{2\pi}\int_{-1}^{+1}\frac{\exp(\frac{\gamma_b}{x-1})}{\sqrt{1-x^2}}\,dx$
Non-Coherent Modulation			
MDPSK		$P_s = \frac{\sin\frac{\pi}{M}}{\pi}$ $\int_0^{\frac{\pi}{2}}\frac{\exp[-\log(M)\gamma_b(1-\cos(\frac{\pi}{M}\cos\theta))]}{1-\cos\frac{\pi}{M}\cos\theta}\,d\theta$	$P_s = \frac{\sin\frac{\pi}{M}}{2\pi}$ $\int_{-1}^{+1}\frac{\frac{\exp[-\log(M)(1-\cos\frac{\pi}{M}\cos(\frac{1}{2}\cos^{-1}x))\gamma_b]}{1-\cos\frac{\pi}{M}(\cos(\frac{1}{2}\cos^{-1}x))}}{\sqrt{1-x^2}}\,dx$
$\pi/4$-DQPSK		$P_s = \frac{1}{2\pi}\int_0^{\pi}\exp\left(-\frac{2\gamma_b}{2-\sqrt{2}\cos\theta}\right)d\theta$	$P_s = \frac{1}{2\pi}\int_{-1}^{+1}\frac{\exp\left(-\frac{2\gamma_b}{2-\sqrt{2}x}\right)}{\sqrt{1-x^2}}$

3.5 Numerical and Simulation Results

In this section, classical and rational GCQ rules are used for evaluating SER in both single and diversity receptions over the Rayleigh, Rician and Nakagami-m fading channels. The MGF approach of calculating the average error rate is adopted.

3.5.1 Error Performance of Single Channel Reception

Numerical results for several digital modulation schemes are provided to investigate the efficiency of both classical and rational GCQ rules. An excellent agreement between the analytical and numerical integration simulation results is observed.

Rayleigh Fading

Figures 3.12-3.16 show the performance of different digital modulation schemes described in Section 3.4 in the single channel reception over Rayleigh fading scenario. The average BERs/SERs are quantified by both classical and rational GCQ rules. For comparison, the exact average BERs/SERs are generated through numerical integrations.

Subfigures 3.12-3.16 (a) show the exact BERs/SERs of several digital modulation schemes and the quantified BERs/SERs by adopting the classical and rational GCQ rules with 2 nodes. These subfigures show that the rational GCQ outperforms the classical GCQ rule in the low SNR region.

Subfigures 3.12-3.16 (b) show the number of $nodes$ required for each method to converge. The convergence rate is defined by

$$\lim_{m \to \infty} \frac{v_m - v_{m-1}}{v_m} \leq 10^{-5}, \tag{3.62}$$

where m refers to the number of $nodes$, and v refers to the relative error, which is determined by the number of $nodes$. By comparing the relative error obtained through the number of $nodes$ and its adjacent number of $(nodes - 1)$ at the same SNR in the region of less or equal than 10^{-5}, the minimal required m can be obtained. It is clear that rational GCQ rule converges faster than the classical GCQ rule in the lower SNR region.
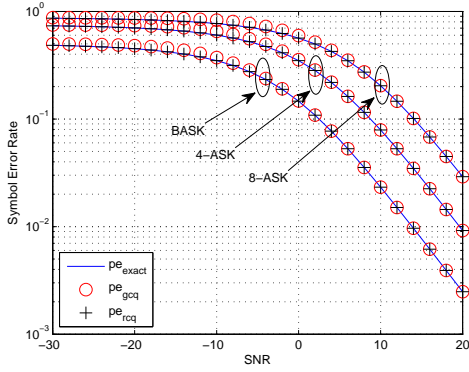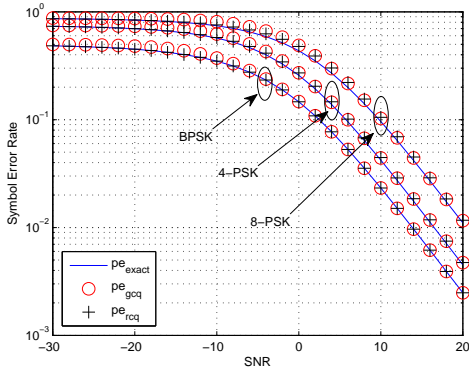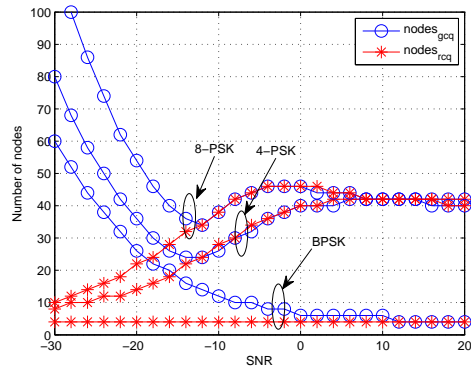
(a) Error performance with 2 nodes
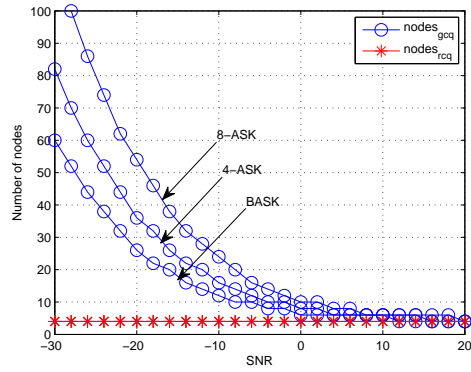
(b) Convergence rate of GCQ

Figure 3.12: Coherent Detection of M-ary ASK ($M = 2, 4, 8$) in Rayleigh fading
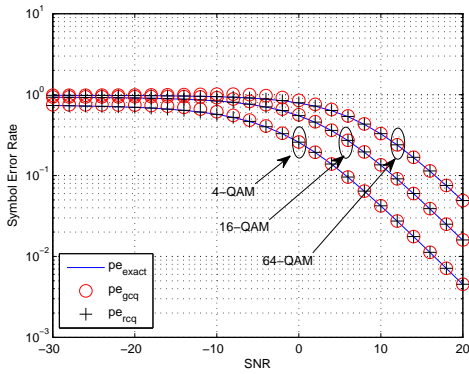

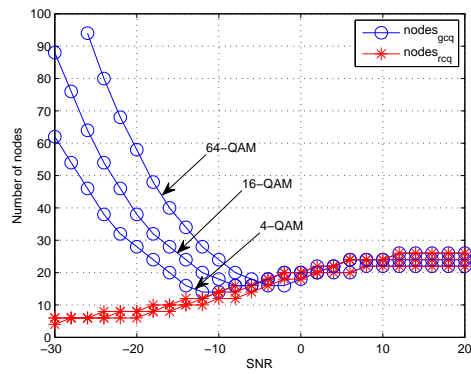
(a) Error performance with 2 nodes

(b) Convergence rate of GCQ

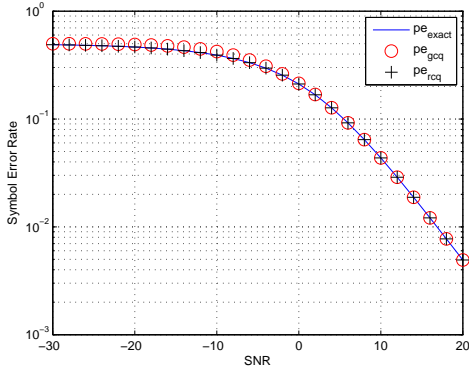Figure 3.13: Coherent Detection of M-ary PSK ($M = 2, 4, 8$) in Rayleigh fading

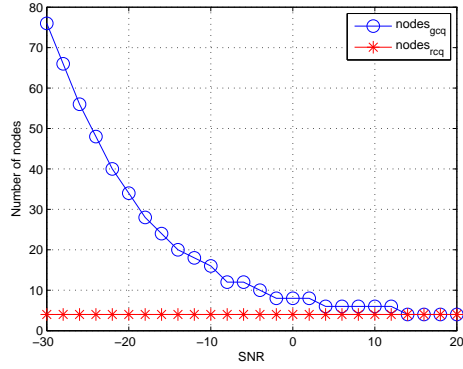
(a) Error performance with 2 nodes

(b) Convergence rate of GCQ

Figure 3.14: Coherent Detection of M-ary QAM ($M = 4, 16, 64$) in Rayleigh fading
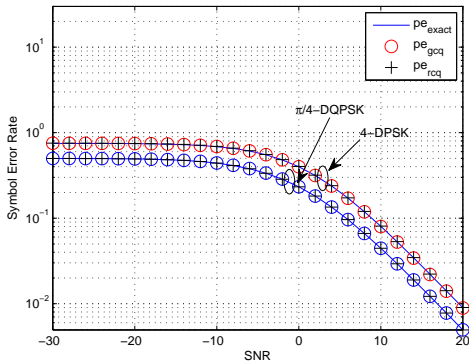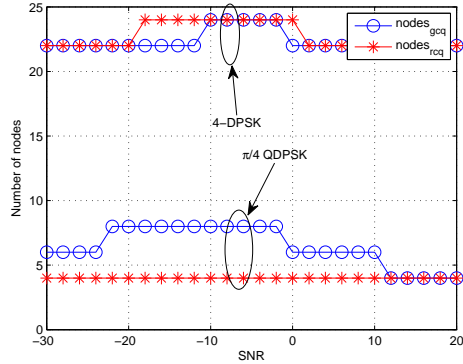
44

(a) Error performance with 2 nodes

(b) Convergence rate of GCQ

Figure 3.15: Coherent Detection of BFSK in Rayleigh fading

(a) Error performance with 2 nodes

(b) Convergence rate of GCQ

Figure 3.16: Non Coherent Detection of 4-ary DPSK and $\pi/4$-DQPSK modulation in Rayleigh fading

Rician Fading

Figures 3.17-3.21 show the SER of several digital modulations in Rician fading ($K = 3$). It can be seen that in each different digital modulation scheme, the rational GCQ performs better than the classical GCQ rule, especially, in the low SNR region. These figures also show that the rational GCQ rule converges faster than classical GCQ rule; i.e., rational GCQ requires fewer $nodes$ than the classical one, where the convergence rate is defined as the same as it is in the numerical analysis shown in Rayleigh fading.
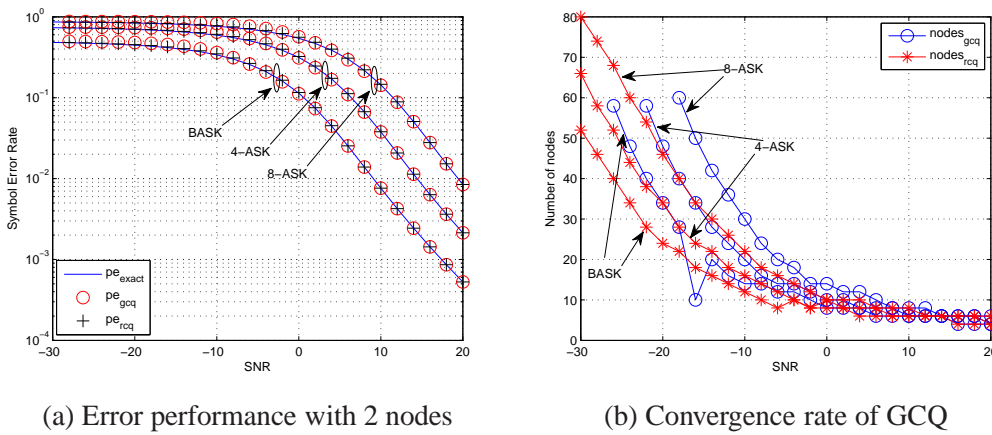

(a) Error performance with 2 nodes

(b) Convergence rate of GCQ

Figure 3.17: Coherent Detection of M-ary ASK ($M = 2, 4, 8$) in Rician fading ($K = 3$).

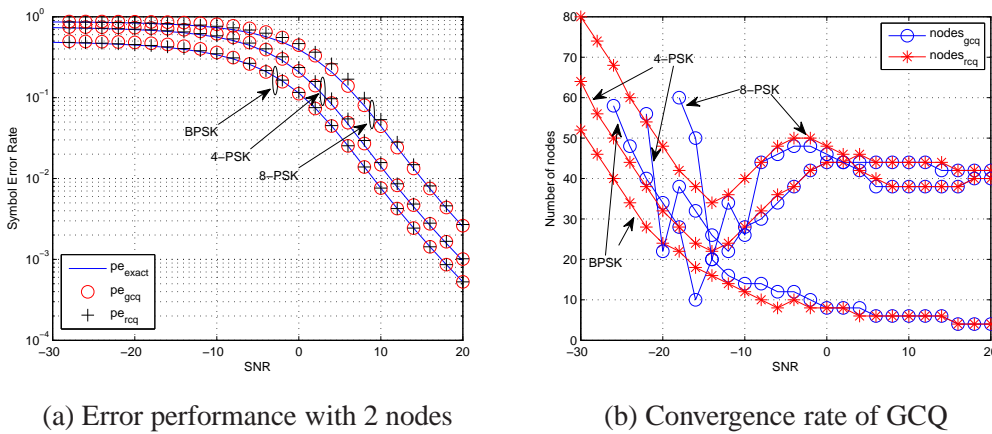(a) Error performance with 2 nodes
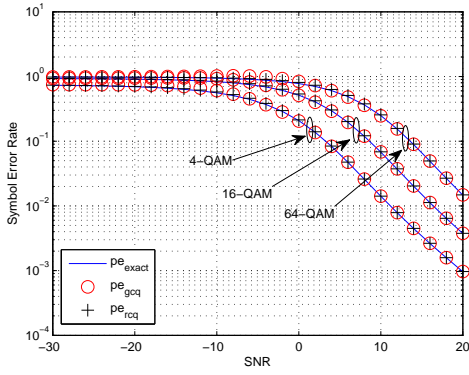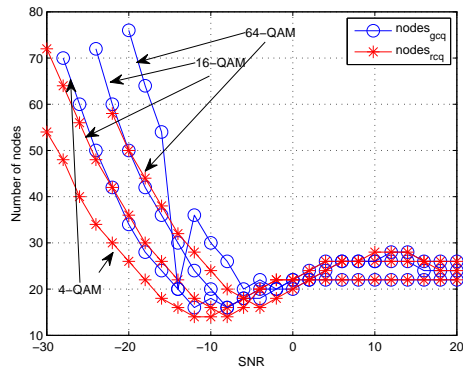
(b) Convergence rate of GCQ

Figure 3.18: Coherent Detection of M-ary PSK ($M = 2, 4, 8$) in Rician fading ($K = 3$).
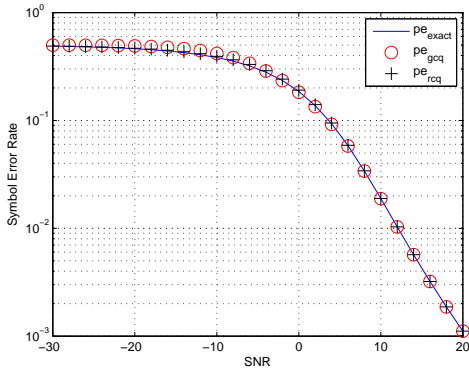
(a) Error performance with 2 nodes

(b) Convergence rate of GCQ

Figure 3.19: Coherent Detection of M-ary QAM ($M = 4, 16, 64$) in Rician fading ($K = 3$).

(a) Error performance with 2 nodes

(b) Convergence rate of GCQ

Figure 3.20: Coherent Detection of BFSK in Rician fading ($K = 3$).

(a) Error performance with 2 nodes

(b) Convergence rate of GCQ

Figure 3.21: Non Coherent Detection of 4-ary DPSK and $\pi/4$-DQPSK in Rician fading ($K = 3$).

Nakagami-2 Fading

The error performance of different digital modulations in Nakagami-2 fading is presented in Figures 3.22-3.26. The rational GCQ rule has a relatively lower error in the low SNR region, and its convergence rate is better than that of the classical GCQ rule.

(a) Error performance with 2 nodes   (b) Convergence rate of GCQ

Figure 3.22: Coherent Detection of M-ary ASK ($M = 2, 4, 8$) in Nakagami-2 fading
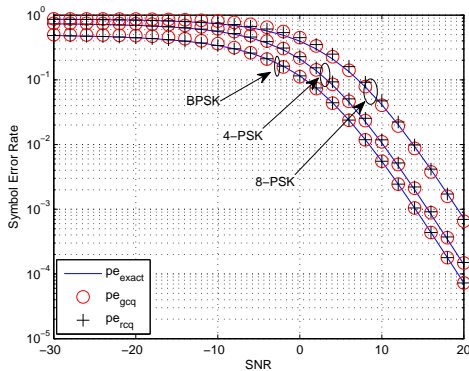
(a) Error performance with 2 nodes   (b) Convergence rate of GCQ

Figure 3.23: Coherent Detection of M-ary PSK ($M = 2, 4, 8$) in Nakagami-2 fading
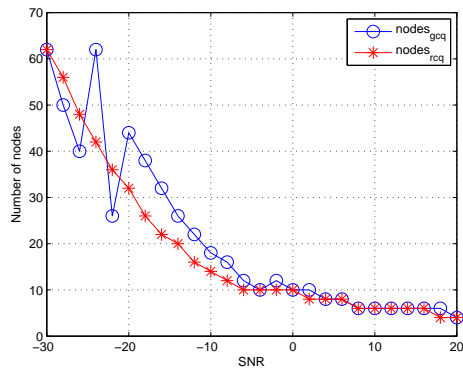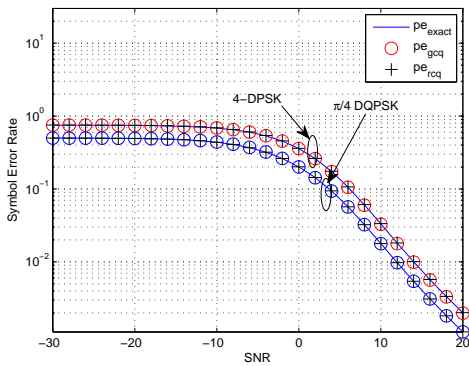
(a) Error performance with 2 nodes

(b) Convergence rate of GCQ

Figure 3.24: Coherent Detection of M-ary QAM ($M = 4, 16, 64$) in Nakagami-2 fading
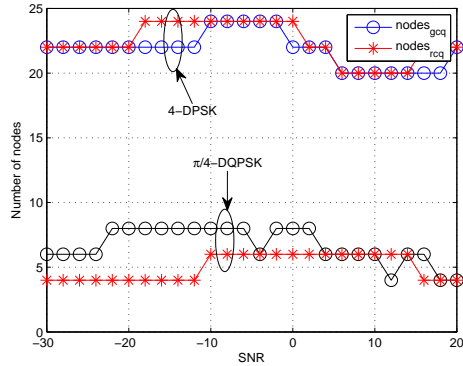

(a) Error performance with 2 nodes

(b) Convergence rate of GCQ

Figure 3.25: Coherent Detection of BFSK in Nakagami-2 fading

(a) Error performance with 2 nodes

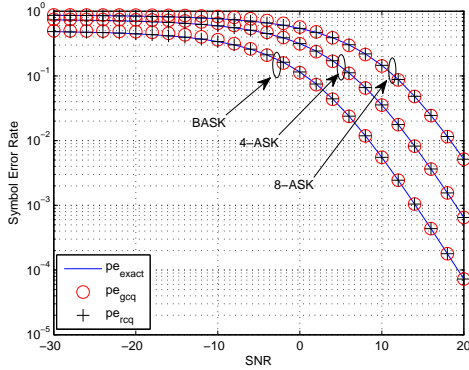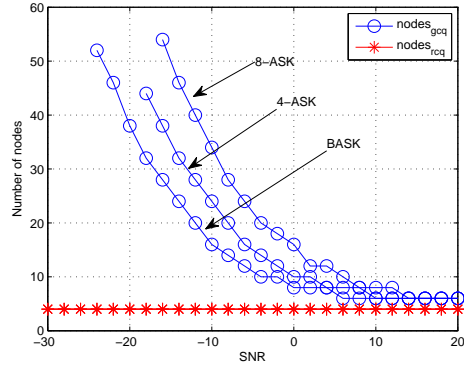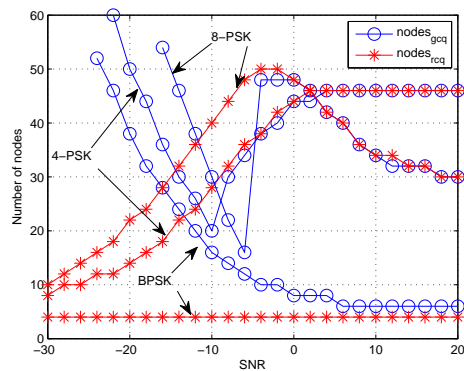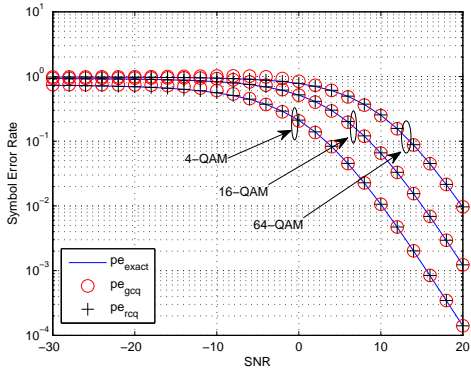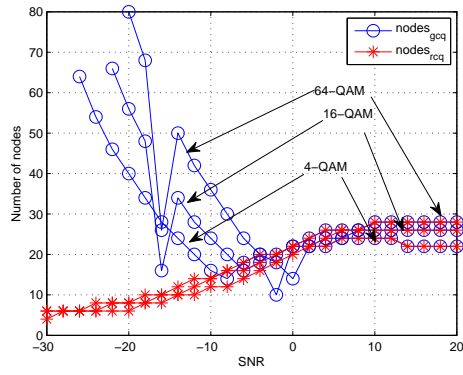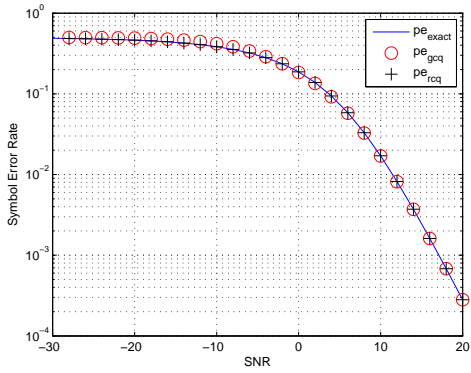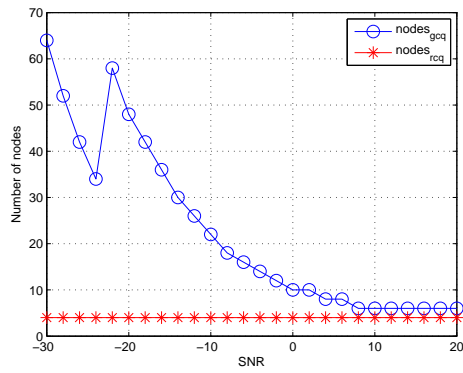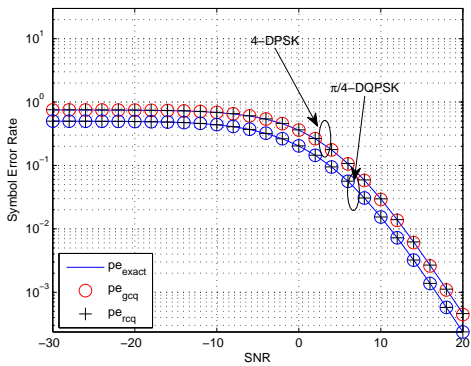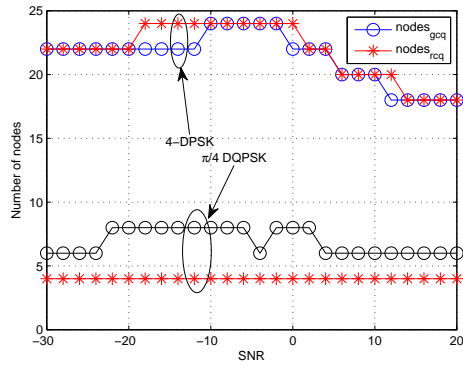(b) Convergence rate of GCQ

Figure 3.26: Non Coherent Detection of M-ary DPSK and $\pi/4$-DQPSK in Nakagami-2 fading

3.5.2 Error Performance of Diversity Reception

The three commonly used diversity combining techniques are maximal ratio combining (MRC), equal gain combining (EGC), and selection combining (SC). Here, we will focus on only MRC. MRC is an optimal diversity combining technique for the independent AWGN channels since MRC provides the highest average output SNR regardless of the fading statistics [48]. The MGF of the SNR in MRC can be expressed as

$$\varphi_\gamma(s) = \mathbb{E}[\exp[-s(\gamma_1 + \gamma_2 + \ldots + \gamma_L)]]$$
$$= \prod_{l=1}^{L} \varphi_{\gamma_l}(s) \tag{3.63}$$

where L is the number of diversity branches. Thus, the MRC case for digital modulation schemes can be obtained by combining Table 3.1 and the MGF of the SNR over different fading scenarios.

Recognizing that the CEP of M-ary PSK in Table 3.1 has a common format, we can intuitively derive every single angle from it. Thus, we will use M-ary PSK as a proxy for general digital modulation schemes to investigate the rational GCQ in different common fadings.

Rayleigh Fading

Figure 3.27 shows the SERs of 8-PSK with the assumption that all the MRC space diversity branches undergo identical Rayleigh fading. The exact performance curve of MRC is generated by using the numerical integration simulation. Figure 3.27 reveals that the difference between rational GCQ and classical GCQ rules is quite small .

Figures 3.28, 3.29, and 3.30 compare the convergence rate as ($nodes \to \infty$) of the classical and rational GCQ rules for Rayleigh fading channels. These figures show that as the diversity order L increases the absolute error, $|P_{exact} - P_{gcq}|$, is decreasing. In other words, MRC provides the best combination of SER of any of the modulation schemes. This result is to be expected because diversity reception implements an effective technique for suppressing the channel fading effects. As

the *nodes* increase, both classical GCQ and rational GCQ turn to be equivalent. Another observation is that by using a small number of *nodes* for both classical and rational GCQ rules for evaluation, rational GCQ rule has a lower value of the absolute error, so that the rational GCQ rule has a better convergence rate.

Table 3.2 shows the required number of *nodes* for classical and rational GCQ rules and their relative error. One recognition is that in the low SNR region, the rational GCQ requires fewer *nodes* to converge, and the relative error is smaller than that of the classical GCQ rule. In the high SNR region, the rational GCQ and the classical GCQ require almost an equal number of *nodes* to converge, and the relative error for each is almost the same. However, when the number of *nodes* is smaller, the rational GCQ performs better than the classical GCQ.

Figure 3.27: Error performance for 8PSK with diversity reception in Rayleigh fading ($nodes = 8$).

51

Figure 3.28: Error performance for 8PSK with MRC ($L = 1$) in Rayleigh fading.

Figure 3.29: Error performance for 8PSK with MRC ($L = 2$) in Rayleigh fading.

Figure 3.30: Error performance for 8PSK with MRC ($L = 3$) in Rayleigh fading.

Table 3.2: Relative errors:$L = 1, 2, 3$, MRC, Rayleigh fading

Average SNR	L	number of nodes		Relative Error	
γ_b		nodes_{gcq}	nodes_{rcq}	relative error$_{gcq}$	relative error$_{rcq}$
-20 dB	1	54	22	2.78e-05	3.56e-05
	2	56	28	5.52e-05	4.75e-05
	3	44	32	1.41e-04	5.69e-05
-10 dB	1	38	38	7.97e-05	8.35e-05
	2	46	48	1.03e-04	1.02e-04
	3	50	52	1.09e-04	1.12e-04
0 dB	1	46	46	9.85e-05	1.01e-04
	2	40	42	8.41e-05	8.20e-05
	3	30	32	5.96e-05	6.05e-05
10 dB	1	42	42	8.92e-05	9.05e-05
	2	10	10	5.77e-05	6.14e-05
	3	10	12	2.31e-06	2.36e-06
20 dB	1	40	40	9.07e-05	9.11e-05
	2	10	10	2.17e-05	2.22e-05
	3	10	10	5.06e-07	5.02e-07

Rician Fading

Figure 3.31 compares the SER of 8-PSK with MRC reception in identical Rician fading, where the Rician fading factor $K = 3$. One recognition is that SER evaluation using rational and classical GCQ rules is quite close to the exact performance. Figure 3.32, 3.33, and 3.34 compare the convergence rate as ($nodes \to \infty$) of the classical GCQ and rational GCQ rules for Rician fading ($K = 3$) channel. It can be seen that as the diversity order L increases, the evaluation of the absolute errors between classical and rational rules is decreasing. This result verifies that MRC is an effective diversity combining technique.

In Table 3.3, selected data of the required number of $nodes$ and relative error between the classical GCQ and rational GCQ rules are presented. This table reveals that in the low SNR region, the required number of $nodes$ and the relative errors of rational GCQ are smaller than those of the classical GCQ rule. In the high SNR region, the number of $nodes$ required to converge and the relative errors are similar, except when $\gamma_b = -10$ dB, $L = 1$ and $\gamma_b = 20$ dB, $L = 3$. These two exceptions are caused by the convergence rate. The classical GCQ rule converges faster than the rational GCQ in these two exceptional points. However, compared to the results of the relative error, the rational GCQ rule has a high accuracy at these two exceptions.
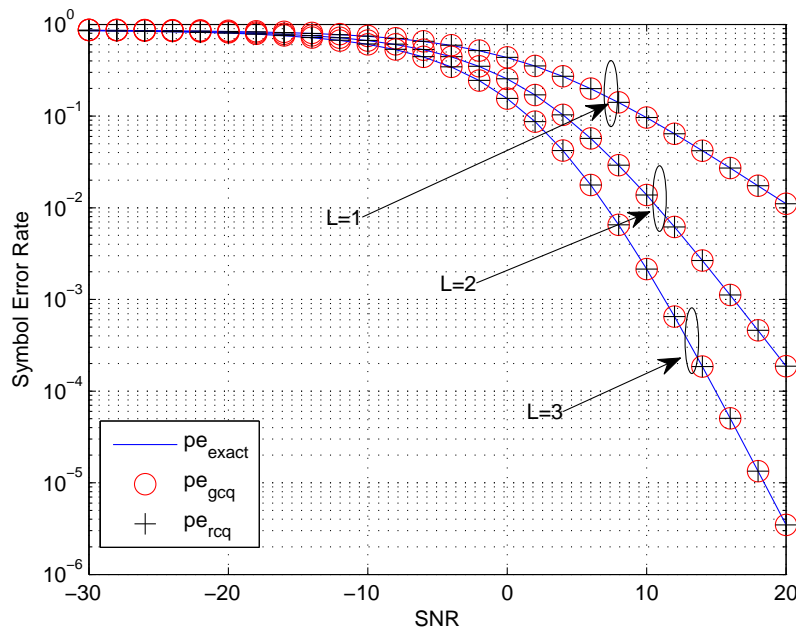

Figure 3.31: Error performance for 8PSK with diversity reception in Rician fading ($K = 3$) and ($nodes = 8$).
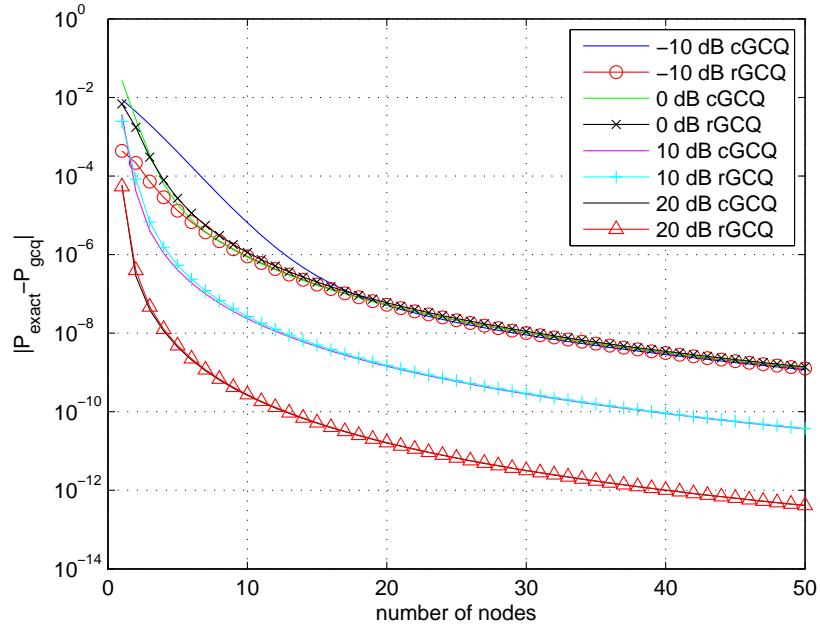
Figure 3.32: Error performance for 8PSK with MRC ($L = 1$) in Rician fading ($K = 3$).
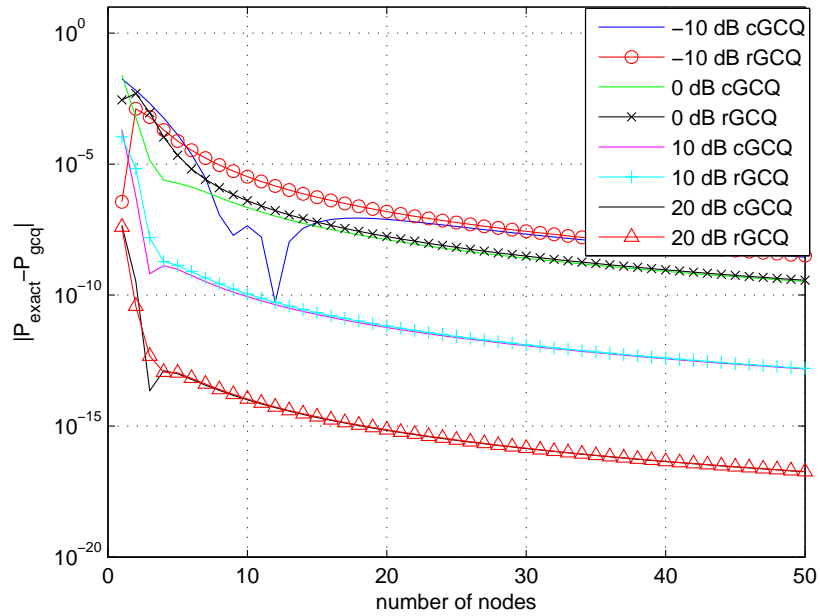

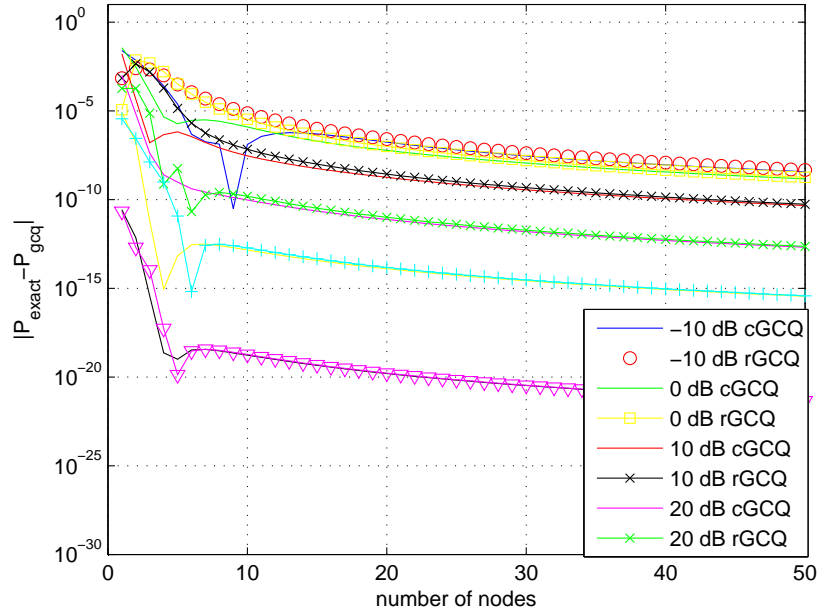Figure 3.33: Error performance for 8PSK with MRC ($L = 2$) in Rician fading ($K = 3$).

Figure 3.34: Error performance for 8PSK with MRC ($L = 3$) in Rician fading ($K = 3$).

Table 3.3: Relative errors:$L = 1, 2, 3$, MRC, Rician fading and Rician factor $K = 3$

Average SNR	L	number of nodes		Relative Error	
γ_b		nodes$_{gcq}$	nodes$_{rcq}$	relative error$_{gcq}$	relative error$_{rcq}$
-20 dB	1	38	48	4.56e-04	2.71e-05
	2	54	38	5.94e-05	4.11e-05
	3	44	36	1.48e-04	5.10e-05
-10 dB	1	26	40	1.78e-04	8.56e-05
	2	46	48	1.04e-04	1.04e-04
	3	50	52	1.10e-04	1.14e-04
0 dB	1	46	48	1.07e-04	1.02e-04
	2	40	40	8.05e-05	8.75e-05
	3	30	32	5.65e-05	5.82e-05
10 dB	1	38	38	7.52e-05	7.73e-05
	2	22	24	4.92e-05	4.53e-05
	3	10	12	2.41e-05	2.29e-05
20 dB	1	40	40	8.32e-05	8.41e-05
	2	28	28	5.74e-05	5.91e-05
	3	8	18	1.03e-04	3.18e-05

Nakagami-m Fading

Figure 3.35 shows the SERs evaluation of Nakagami-m ($m = 2$) with the MRC diversity branches undergoing identical Nakagami-2 fading. Figure 3.36,3.37, and 3.38 compare the convergence rate as ($nodes \to \infty$) of the classical GCQ and rational GCQ rules for Nakagami-2 fading.

In Table 3.4, selected data for the required number of $nodes$ and the relative errors for classical GCQ and rational GCQ rules are illustrated. In the low SNR region, the rational GCQ rule needs fewer $nodes$ to converge, and the relative error is almost 10 times less than that of the classical GCQ; i.e., rational GCQ rule has high accuracy. In the high SNR region, the number of $nodes$ required for convergence and the relative errors is almost the same, except for the $\gamma_b = -10$ dB, $L = 1$ and $\gamma_b = 20$ dB, $L = 3$. These two exceptions are caused by the convergence rate. The classical GCQ rule converges faster than the rational GCQ at these two exceptional points. However, compared to the results for the relative error, those for the rational GCQ rule have high accuracy at these two exceptions.
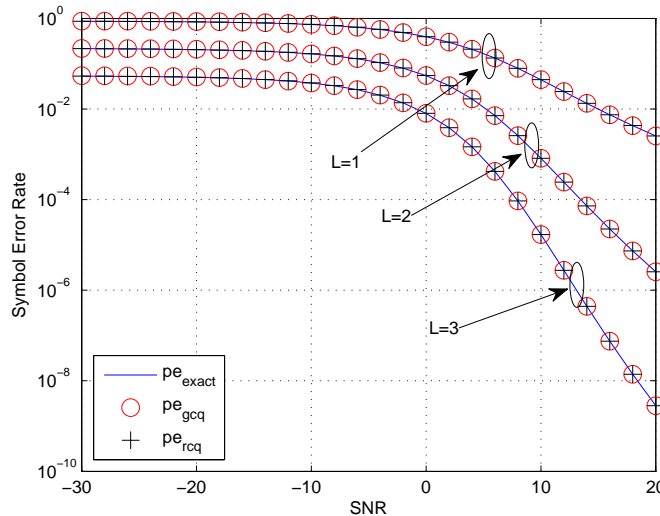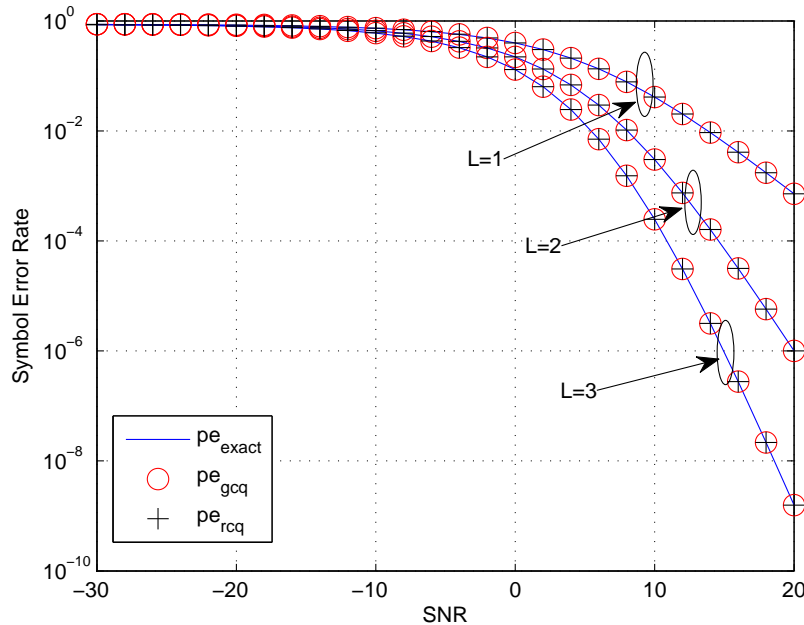

Figure 3.35: Error performance for 8PSK with diversity reception in Nakagami-2 fading ($nodes = 8$).
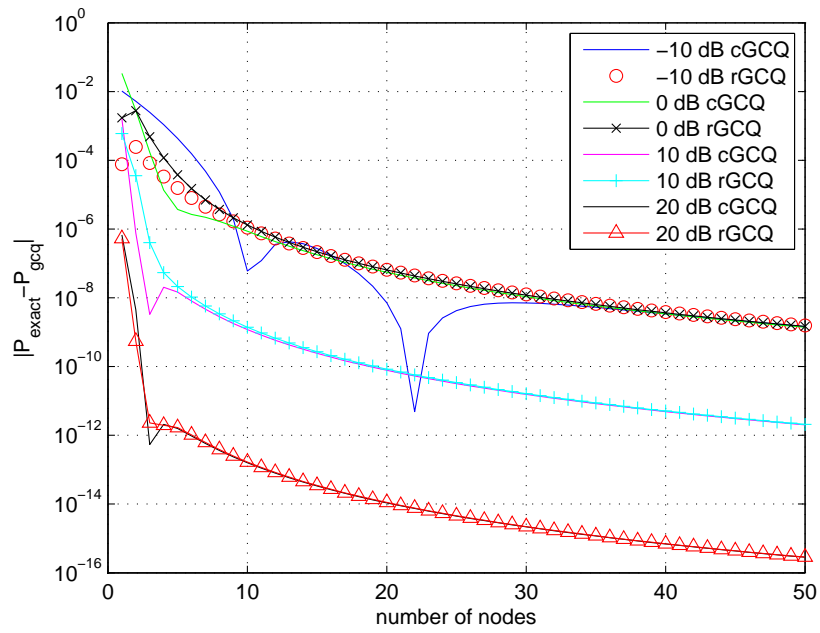
Figure 3.36: Error performance for 8PSK with MRC ($L = 1$) in Nakagami-2 fading.
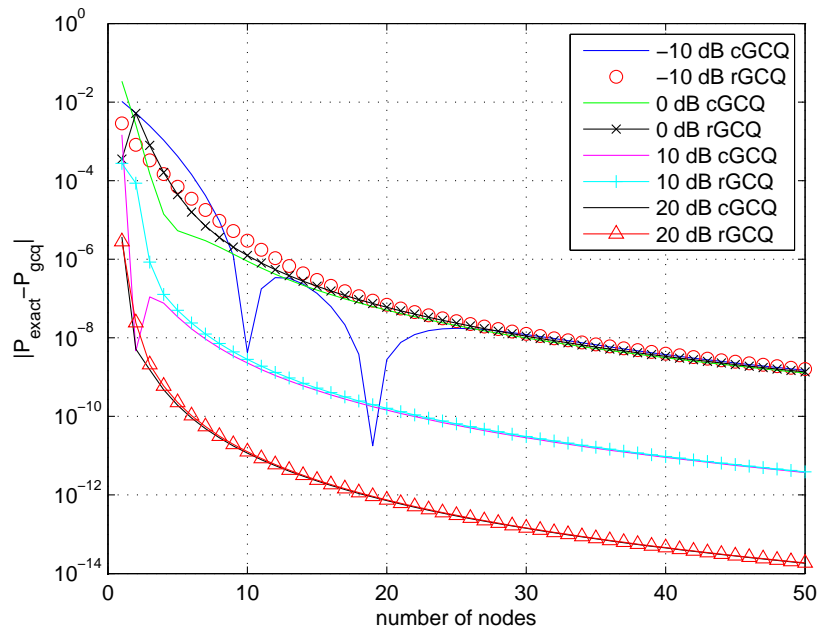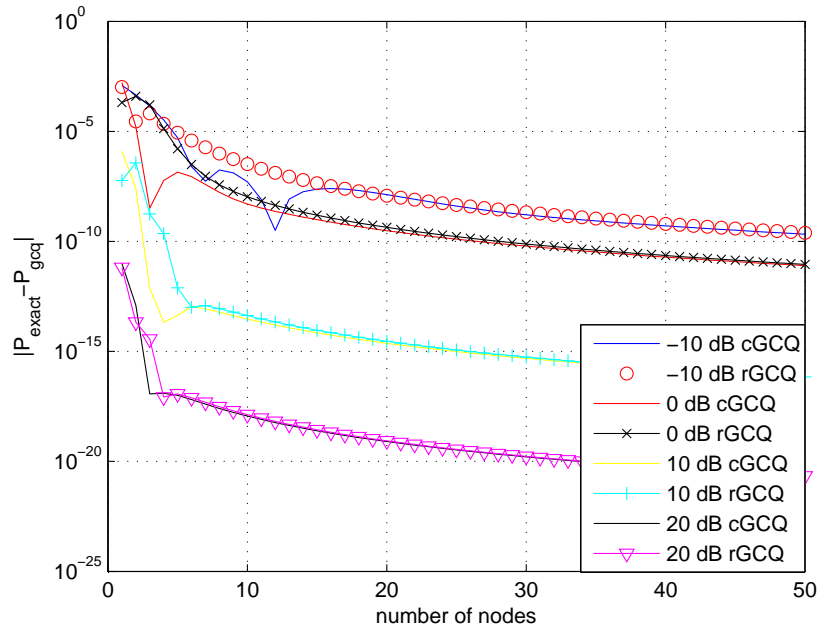

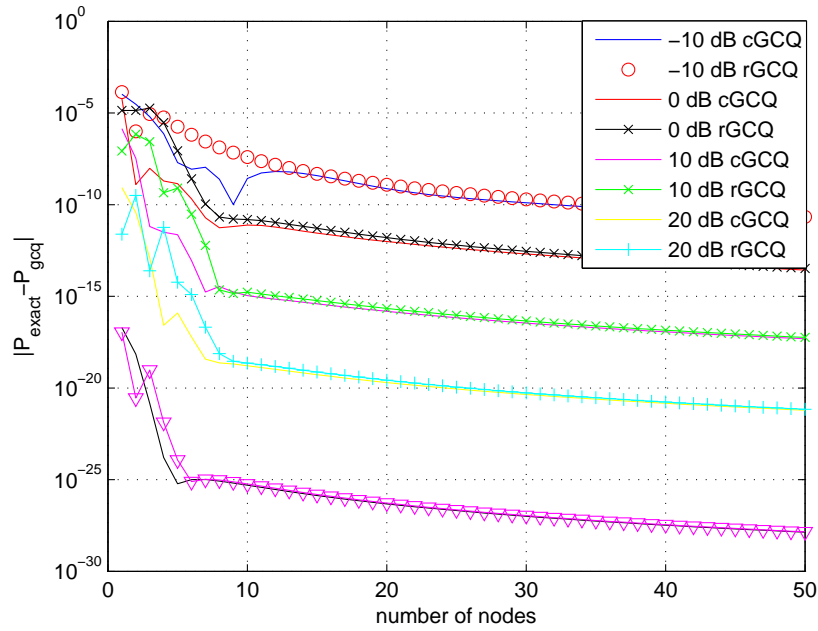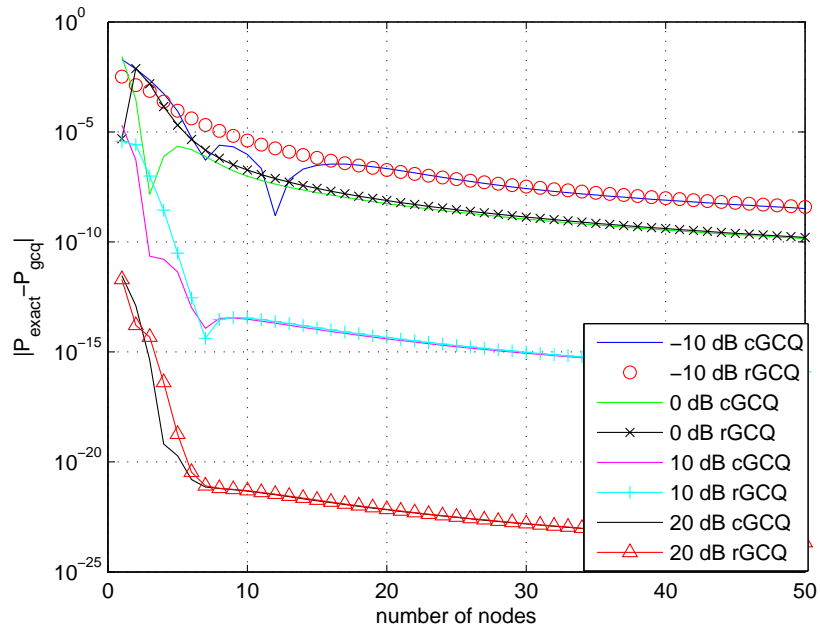Figure 3.37: Error performance for 8PSK with MRC ($L = 2$) in Nakagami-2 fading ($m = 2$).
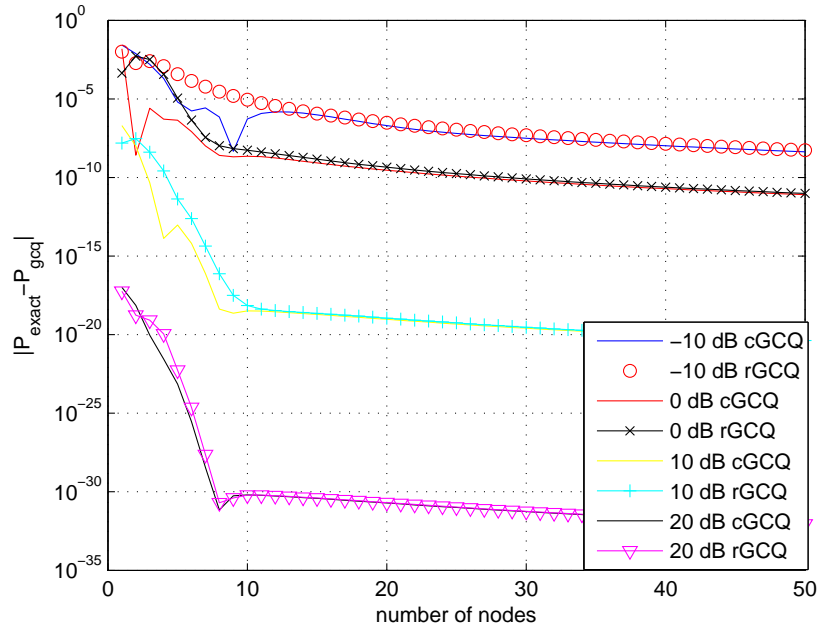
Figure 3.38: Error performance for 8PSK with MRC ($L = 3$) in Nakagami-2 fading ($m = 2$).

Table 3.4: Relative errors: $L = 1, 2, 3$, MRC, Nakagami-2 fading

Average SNR	L	number of nodes		Relative Error	
γ_b		nodes$_{gcq}$	nodes$_{rcq}$	relative error$_{gcq}$	relative error$_{rcq}$
-20 dB	1	40	22	4.56e-04	3.63e-05
	2	58	28	2.62e-05	4.67e-05
	3	48	32	3.75e-05	5.59e-05
-10 dB	1	30	40	1.15e-04	8.45e-05
	2	44	46	1.02e-04	1.01e-04
	3	48	52	1.09e-04	1.03e-04
0 dB	1	48	48	1.02e-04	1.05e-04
	2	44	44	9.25e-05	9.83e-05
	3	38	40	7.58e-05	7.57e-05
10 dB	1	34	34	7.41e-05	7.59e-05
	2	32	34	6.34e-05	6.54e-05
	3	22	22	4.36e-05	4.73e-05
20 dB	1	30	30	6.47e-05	6.53e-05
	2	30	30	6.29e-05	6.38e-05
	3	20	8	3.61e-05	1.62e-04

3.6 Conclusion

This chapter reviewed the performance of coherent and noncoherent digital modulation schemes over typical multipath fading channels. Analytical expressions of BER/SER were tabulated for the cases where the classical and rational GCQ rules can be adopted. One new generalized integral model for adopting rational GCQ rule, i.e., SER of M-PSK, with arbitrary upper limits was investigated. Numerical results showed that in the low SNR region, the rational GCQ rule provided a rapid convergence rate and better accuracy than the classical GCQ rule. In the high SNR region, the classical and rational GCQ rules had almost the same performance. However, when the number of nodes was smaller, i.e., less than the number required for each rule to converge, the rational GCQ performed better than the classical GCQ.

$\sim$

Chapter 4

GCQ for Co-Channel Interference Outage

In Chapter 3, performance metrics of SER over multipath fading channels were described. This chapter will use GCQ rules for computing the outage.

4.1 Introduction

In this chapter, the use of classical and rational GCQ rules for outage probability analysis in the presence of CCI is investigated. Numerical examples of unequal Rice factors and transmit powers over the Rayleigh and Rician fading distributions demonstrate the high accuracy of these methods.

In the remainder of this chapter, outage computation and the desired form of GCQ rule for calculating outage probability of each different fading case is illustrated in Section 4.2. Numerical and simulation examples are presented in Section 4.3. Finally, Section 4.4 concludes the chapter.

4.2 Outage Probability

The outage probability, P_{out}, is defined as the probability that the instantaneous SIR falls below a certain threshold value. The outage probability of an interference-limited network can be expressed as

$$P_{out} = \mathbb{P}\{\Omega_0 < \gamma_{th}(\Omega_1 + \ldots + \Omega_L)\}, \tag{4.1}$$

where Ω_0 and $\Omega_1, \ldots, \Omega_L$ are the instantaneous signal powers of the desired signal and interfering signals, respectively, with average power, $\bar{\Omega}_l$, $l = 0, 1, \ldots, L$. The power protection ratio, γ_{th}, is fixed by the type of modulation and transmission technique employed and the quality of service desired.

The instantaneous SIR is given by

$$\Gamma = \frac{\Omega_0}{\Omega_1 + \ldots + \Omega_L} = \frac{\Omega_0}{\sum_{l=1}^{L} \Omega_l}, \tag{4.2}$$

where the instantaneous SIR falls below a pre-defined threshold γ_{th}. It is easy to show that the outage probability in terms of Γ and γ_{th} is presented as

$$P_{out} = \mathbb{P}(\Gamma < \gamma_{th}). \tag{4.3}$$

Let us define a new variable γ_{SIR}:

$$\gamma_{SIR} = \Gamma - \gamma_{th}$$
$$= \frac{\Omega_0}{\gamma_{th}} - \sum_{l=1}^{L} \Omega_l. \tag{4.4}$$

The MGF of γ_{SIR} is given by

$$\varphi_{\gamma_{SIR}} = \varphi_0(\frac{s}{\gamma_{th}}) \prod_{l=1}^{L} \varphi_l(-s), \tag{4.5}$$

where φ_l is the MGF of p_l and can be any one of the MGFs in Section 3.2. It follows that the outage probability is given by

$$P_{out} = \mathbb{P}(\gamma_{SIR} < 0). \tag{4.6}$$

P_{out} can also be written as [49]

$$P_{out} = \frac{1}{2\pi} \int_{-\infty}^{\infty} \frac{\varphi_{\gamma_{SIR}}(c + jw)}{c + jw} dw$$
$$= \frac{1}{\pi} \int_{0}^{\infty} \frac{\mathrm{Re}[(c - jw)(\varphi_{\gamma_{SIR}}(c + jw))]}{c^2 + w^2} dw, \tag{4.7}$$

where $j^2 = -1$, $0 < c < s_{min} = min\{s_i | 1 \leq i \leq L\}$ with s_i being the i-th pole of $\varphi_{\gamma_{SIR}}(s)$ in the right-half plane. Although the value of c can be selected anywhere between 0 and s_{min}, it is better to choose it such that $\varphi_{\gamma_{SIR}}$ decays very rapidly as $w \to \infty$. In practice, it is sufficient to use $c = s_{min}/2$ [18, 49].

By substituting $w = c\tan(\theta/2)$ into (4.7), we get [18]

$$P_{out} = \frac{1}{2\pi} \int_0^\pi \mathrm{Re}[(1 - j\tan(\frac{\theta}{2}))(\varphi_{\gamma_{SIR}}(c + jc\tan(\frac{\theta}{2})))]\, d\theta. \qquad (4.8)$$

Further, by using variable substitution $x = \cos\theta$ in (4.8), we get [2]

$$P_{out} = \frac{1}{2\pi} \int_{-1}^{+1} \frac{\mathrm{Re}\left\{\left(1 - j\frac{\sqrt{1-x^2}}{1+x}\right)\varphi_{\gamma_{SIR}}\left(c + jc\frac{\sqrt{1-x^2}}{1+x}\right)\right\}}{\sqrt{1 - x^2}}\, dx, \qquad (4.9)$$

which is the desired form for applying the rational GCQ and classical GCQ rules.

By using the MGF of the corresponding fading scenario, the desired GCQ format of outage probability of each different fading case can be obtained. However, the available models for using both classical and rational GCQ rules are limited to Rayleigh and Rician fading only, since for other fading scenarios, the use of the rational GCQ rule for the nodes computation always involves complex numbers, which do not satisfy the initial assumption that all the nodes are real values.

4.2.1 Rician Fading with Multiple Rayleigh Interferers

In this case, the desired signal experiences Rician fading while L interfering signals are subject to Rayleigh fading. By using the results from (3.5) and (3.7) for Rayleigh and Rician distributions and substituting them into equation (4.5), the desired signal, $\varphi_0(s/\gamma_{th})$, and the interfering signals, $\varphi_l(-s)$, are obtained as

$$\varphi_0(\frac{s}{\gamma_{th}}) = \frac{\exp\left(-\frac{\frac{K\Omega_0 s}{(K+1)\gamma_{th}}}{1 + \frac{\Omega_0}{(K+1)\gamma_{th}}}\right)}{1 + \frac{\Omega_0 s}{(K+1)\gamma_{th}}}, \qquad (4.10)$$

$$\varphi_l(-s) = \frac{1}{(1 - \Omega_l s)}. \qquad (4.11)$$

Therefore, the MGF of γ_{SIR} is

$$\varphi_{\gamma_{SIR}}(s) = \varphi_0(\frac{s}{\gamma_{th}}) \prod_{l=1}^{L} \varphi_l(-s)$$

$$= \frac{\exp\left(-\frac{\frac{K\Omega_0 s}{(K+1)\gamma_{th}}}{1 + \frac{\Omega_0}{(K+1)\gamma_{th}}}\right)}{\left(1 + \frac{\Omega_0 s}{(K+1)\gamma_{th}} \prod_{l=1}^{L}(1 - \Omega_l s)\right)}. \qquad (4.12)$$

The outage can be computed by substituting (4.12) into (4.9). For the rational GCQ rule, the pole of the function $f(x)$ needs to be found first. One observation can

be found is that $f(x)$ has a pole of infinite multiplicity at $-\left(1 + \frac{2\Omega_0^2 c^2/(\gamma_{th}^2(K+1)^2)}{1+2\Omega_0 c/(\gamma_{th}(K+1))}\right)$ and L simple poles at $-\left(1 + \frac{2\Omega_l^2 c^2}{1-2\Omega_l c}\right)$.

4.2.2 Multiple Rician Interferers

In the case of the desired signal and the L interfering signals both experiencing Rician fading, by applying the MGF expression from (3.7), the desired signal, $\varphi_0(s/\gamma_{th})$, and the interfering signals, $\varphi_l(-s)$ are obtained as

$$\varphi_0\left(\frac{s}{\gamma_{th}}\right) = \frac{\exp\left(-\frac{\frac{K_0\Omega_0 s}{(1+K_0)\gamma_{th}}}{1+\frac{\Omega_0 s}{(1+K_0)\gamma_{th}}}\right)}{1+\frac{\Omega_0 s}{(1+K_0)\gamma_{th}}}, \tag{4.13}$$

$$\varphi_l(-s) = \frac{\exp\left(\frac{\frac{K_l\Omega_l s}{1+K_l}}{1-\frac{\Omega_l s}{1+K_l}}\right)}{1-\frac{\Omega_l s}{1+K_l}}. \tag{4.14}$$

The MGF of γ_{SIR} is

$$\varphi_{\gamma_{SIR}}(s) = \frac{\exp\left(-\frac{\frac{K_0\Omega_0 s}{(1+K_0)\gamma_{th}}}{1+\frac{\Omega_0 s}{(1+K_0)\gamma_{th}}}\right)}{1+\frac{\Omega_0 s}{(1+K_0)\gamma_{th}}} \cdot \prod_{l=1}^{L} \frac{\exp\left(\frac{\frac{K_l\Omega_l s}{1+K_l}}{1-\frac{\Omega_l s}{1+K_l}}\right)}{1-\frac{\Omega_l s}{1+K_l}}. \tag{4.15}$$

To compute the outage, we just need to substitute (4.15) into (4.9). By using the rational GCQ rule, the poles of $f(x)$ can be found at one pole of multiplicity at $-\left(1 + \frac{2\Omega_0^2 c^2/(\gamma_{th}(K_0+1))^2}{1+2\Omega_0 c/(\gamma_{th}(K_0+1))}\right)$ and L simple poles at $-\left(1 + \frac{2\Omega_l^2 c^2/((1+K_l)^2)}{1+2\Omega_l c/(1+K_l)}\right)$.

4.2.3 Mixed Rayleigh and Rician Interferers

In this case, the desired signal is subject to Rician fading, and the total number of L interfering signals are composed of both Rayleigh and Rician faded signals; i.e., there are M Rayleigh interferers and $L - M$ Rician interferers. By applying the MGF from (3.5) and (3.7), the corresponding desired signal, $\varphi_0(s/\gamma_{th})$, the interfering signals of Rayleigh fading, $\varphi_m(-s)$, and the interfering signals of Rician

fading, $\varphi_n(-s)$ can be written as

$$\varphi_0\left(\frac{s}{\gamma_{th}}\right) = \frac{\exp\left(-\frac{\frac{K_0\Omega_0 s}{(1+K_0)\gamma_{th}}}{1+\frac{\Omega_0 s}{(1+K_0)\gamma_{th}}}\right)}{1+\frac{\Omega_0 s}{(1+K_0)\gamma_{th}}}, \tag{4.16}$$

$$\varphi_m(-s) = \frac{1}{\Omega_m s}, \tag{4.17}$$

$$\varphi_n(-s) = \frac{\exp\left(\frac{\frac{K_n\Omega_n s}{1+K_n}}{1-\frac{\Omega_n s}{1+K_n}}\right)}{1-\frac{\Omega_n s}{1+K_n}}. \tag{4.18}$$

Therefore, the MGF of γ_{SIR} is given by

$$\varphi_{\gamma_{SIR}}(s) = \frac{\exp\left(-\frac{\frac{K_0\Omega_0 s}{(1+K_0)\gamma_{th}}}{1+\frac{\Omega_0 s}{(1+K_0)\gamma_{th}}}\right)}{1+\frac{\Omega_0 s}{(1+K_0)\gamma_{th}}} \cdot \frac{1}{\prod_{m=1}^{M}(1-\Omega_m s)} \cdot \prod_{n=M+1}^{L} \frac{\exp\left(\frac{\frac{K_n\Omega_n s}{1+K_n}}{1-\frac{\Omega_n s}{1+K_n}}\right)}{1-\frac{\Omega_n s}{1+K_n}}. \tag{4.19}$$

The outage can be computed by substituting (4.19) into (4.9). By adopting the rational GCQ approximation, the poles of $f(x)$ can be found. There is one pole located at $-\left(1+\frac{2\Omega_0^2 c^2/(\gamma_{th}(K_0+1))^2}{1+2\Omega_0 c/(\gamma_{th}(K_0+1))}\right)$, M simple poles located at $-\left(1+\frac{2\Omega_m^2 c^2}{1-2\Omega_m c}\right)$, and $L-M$ simple poles located at $-\left(1+\frac{2\Omega_n^2 c^2/((1+K_n)^2)}{1+2\Omega_n c/(1+K_n)}\right)$.

4.3   Numerical Results

In this section, a set of numerical results and simulation examples are provided under the asumption that Rayleigh and Rician fading channels are present. Since the desired format of (4.9) for rational GCQ and classical GCQ rules is straightforward, the main aim is to verify their accuracy, relative error, and convergence rate. In addition, we use the value of $c = s_{min}/2$ as a rule of thumb for the outage computations. For comparison purposes, the exact P_{out} is computed by evaluating (4.8) by using Matlab's $quad8$ function with an absolute tolerance of 10^{-15} [49]. All the investigated cases show excellent agreement between the analytical and simulation results.

4.3.1   Rician Fading with Multiple Rayleigh Interferers

Figure 4.1 shows the outage performance when the desired signal is subject to Rician fading while the interfering signals are Rayleigh faded. The Rician fad-

ing factor of the desired signal $K = 3$, and the number of interferers $L = 2$. The interfering signals' powers are $\bar{\Omega}_l = [1, 1.8]$, and the power protection ratio is $\gamma_{th} = 9.5\,\mathrm{dB}$ [18]. The instantaneous SIR over the power protection ratio $\Lambda = \bar{\Omega}_0/(\gamma_{th} \sum_{l=1}^{L} \bar{\Omega}_l)$. In Figure 4.1 (a), the outage probability values obtained by using the classical GCQ and rational GCQ rules are compared with the exact results. For both GCQ rules, 3 nodes are used. It is apparent from Figure 4.1 (a) that both rules yield highly accurate results. Figure 4.1(b) shows the relative error of each rule. It is clear that rational GCQ rule outperforms the classical GCQ rule with a relatively small number of nodes. In other words, for a given number of nodes, the rational GCQ achieves relatively fewer errors than the classical GCQ rule.

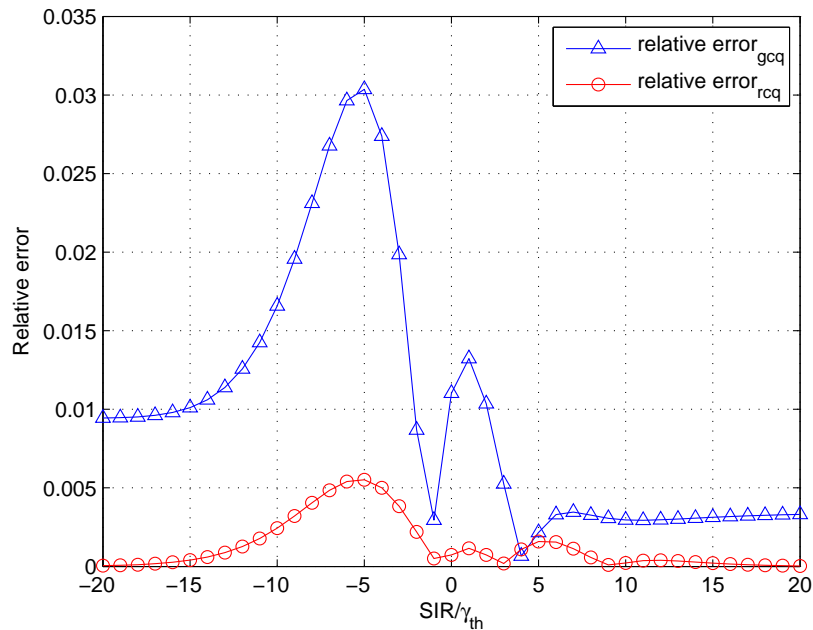## 4.3.2 Rician Fading with Multiple Rician Interferers

Figure 4.2 shows the outage performance when both the desired signal and interfering signals are subject to Rician fading. The Rician fading factor of the desired signal $K = 2$ and the interference signal statistics are given by $L = 2$, $K_l = [1.8, 1.5]$, and $\bar{\Omega}_l = [1, 1.6]$. The power protection ratio $\gamma_{th} = 9.5\,\mathrm{dB}$, and the instantaneous SIR over the power protection ratio $\Lambda = \bar{\Omega}_0/(\gamma_{th} \sum_{l=1}^{L} \bar{\Omega}_l)$. Figure 4.2 (a) shows that both rules yield highly accurate results. Figure 4.2 (b) shows the relative error of each rule. Clearly, rational GCQ rule has better accuracy than the classical GCQ rule, especially in low SIR region. As SIR increases, both methods converge to roughly same levels of relative error.

4.3.3 Rician Fading with Mixed Rayleigh and Rician Interferers

Figure 4.3 illustrates the outage performance when the desired signal is subject to Rician fading and the interfering signals are composed of both Rayleigh and Rician faded signals. The statistics of the given example are $K = 2.8$, $M = 1$, $L = 2$, $K_n = 1.5$, $\bar{\Omega}_l = [1.1, 0.6]$, the power protection ratio is $\gamma_{th} = 9.5\,\mathrm{dB}$, and the instantaneous SIR over the power protection ratio $\Lambda = \bar{\Omega}_0/(\gamma_{th} \sum_{l=1}^{L} \bar{\Omega}_l)$. It is apparent from Figure 4.3 that the rational GCQ approximation yields a better performance in the low SIR region.
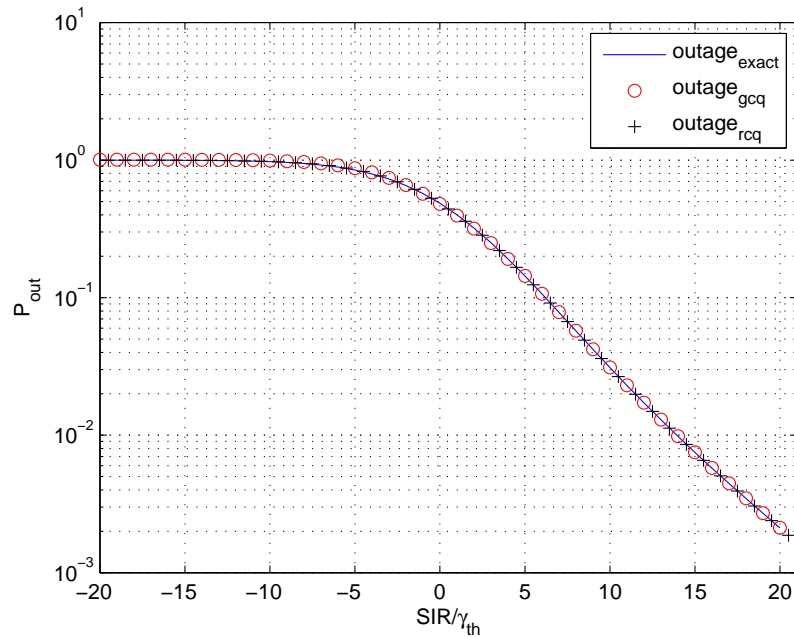
(a) Outage performance versus SIR in a Rician (desired) /Rayleigh (interferer) fading channel with 3 nodes

(b) Relative error versus SIR in a Rician (desired) /Rayleigh (interferer) fading channel with 3 nodes

Figure 4.1: Outage performance of a Rician fading with multiple Rayleigh interferers

(a) Outage performance versus SIR in a Rician (desired) /Rician (interferer) fading channel with 6 nodes

(b) Relative error versus SIR in a Rician (desired) /Rician (interferer) fading channel with 6 nodes

Figure 4.2: Outage performance of a Rician fading with multiple Rician interferers
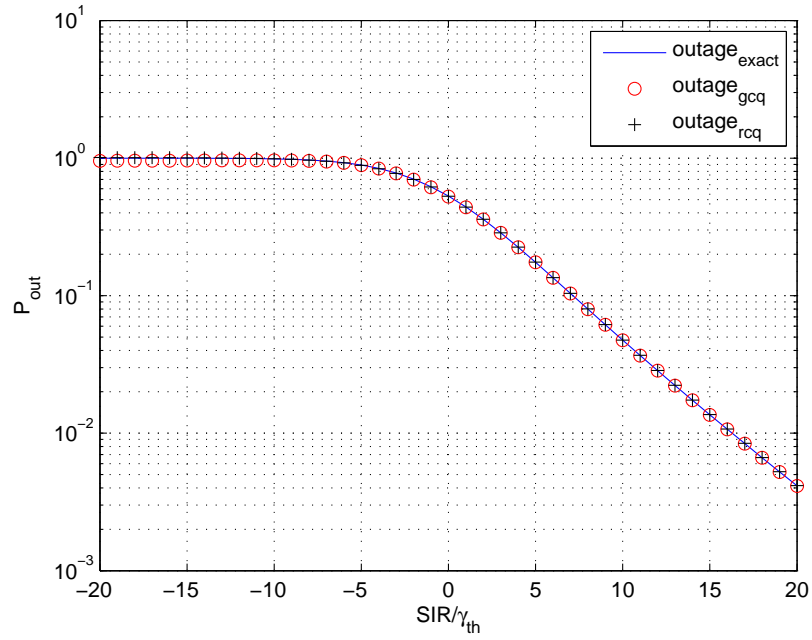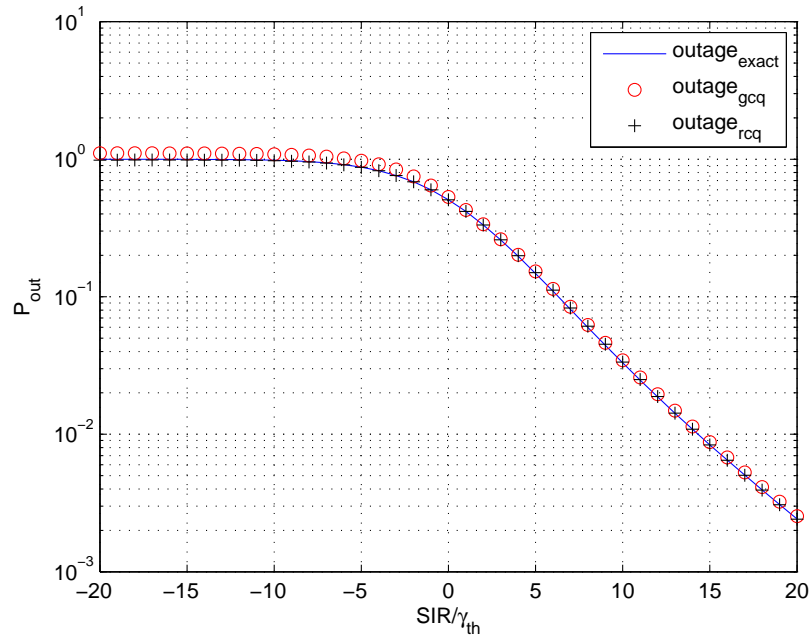
(a) Outage performance versus SIR in a Rician (desired) /Rayleigh and Rician (interferer) fading channel with 4 nodes
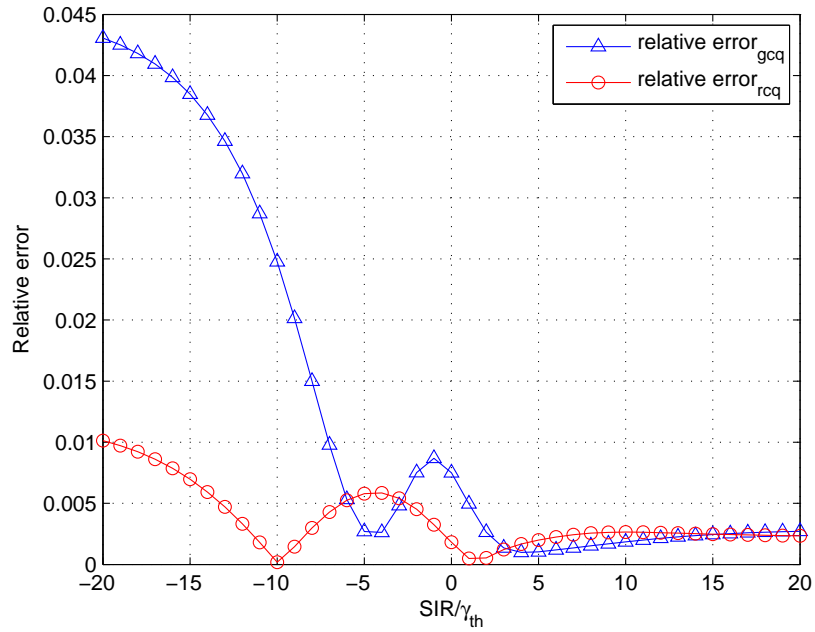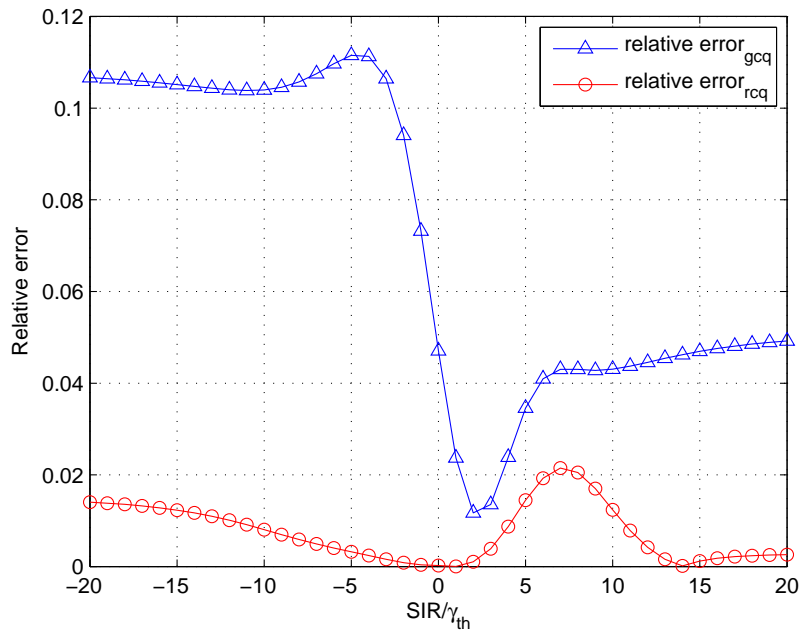

(b) Relative error versus SIR in a Rician (desired) /Rayleigh and Rician (interferer) fading channel with 4 nodes

Figure 4.3: Outage performance of a Rician fading with multiple Rayleigh and Rician interferers

4.4   Conclusion

This chapter presented an exact closed-form expression for the probability of outage in a generalized fading environment. In order to calculate the outage performance, classical GCQ and rational GCQ rules were applied. Since the available modes for using both classical and rational GCQ rules are restricted, all the available cases were listed, i.e., the desired Rician faded signal and aggregate CCIs under Rayleigh or Rician fading or the mix of these two fading scenarios. The simulations results showed that both rules yielded high accuracy. However, when the number of nodes was relatively small, rational GCQ rule always performed better than the classical GCQ rule; i.e., the relative error of rational GCQ was lower than that of classical GCQ rule.

$$\sim$$

Chapter 5

Conclusions

This thesis focused on the relative accuracy of the classical and rational GCQ rules for error performance of digital modulation in the fading and outage performance due to the CCI. These two rules were thus compared in terms of accuracy and complexity. Both rules were shown to provide highly accurate results, and their convergence rate was found to depend on the SNR.

In Chapter 2, several digital modulation techniques and classical and rational GCQ rules were described.

In Chapter 3, classical and rational GCQ rules for SER analysis of coherent and noncoherent detection of different digital modulations in common fading channels were studied. The most significant utilization of those techniques occurred with models for which the closed-form expressions for the error probability were not known. Therefore, in many cases, numerical integration was required to obtain the error probability. Based on these techniques, the closed-form approximations for each modulation were derived. We evaluated the performance of the new technique, rational GCQ, and the conventional technique, classical GCQ, for different digital modulations in multipath fading scenarios. The comparison showed that the rational GCQ had a much more rapid convergence rate and a lower relative error in the low SNR region. Although in the high SNR region, the number of nodes required for convergence was similar, when the number of nodes was less than the number required for convergence, the rational GCQ had a faster rate of convergence.

In Chapter 4, the GCQ formulas were adopted for the outage analysis. The exact closed-form expression for the probability of outage in generalized fading

71

environment was presented. When the desired signal was Rician fading and the interfering signals were Rayleigh or Rician or the combination of those two, the outage expressions were derived.

5.1 Future Research Directions

This thesis work provides a foundation for further research based on the classical and rational GCQ rules. Since the error and outage performance evaluated in this thesis are based on the MGF approach, other fading models and diversity reception methods, where MGF is available, can be evaluated by using GCQ rules [50].

Also, further application of the rational GCQ rule to models with capacity problems may also prove to be useful. In [51, 52], the classical GCQ is successfully applied to analyze of the capacity problem. The rational GCQ can also be used for capacity analysis since the GCQ format is always the same except for the calculation of nodes and weight.

Furthermore, the adopted rational GCQ rule is applicable only when the poles of $f(x)$ are real. In [53], the researchers suggest an algorithm that can be used to calculate the rational GCQ rule when the poles for $f(x)$ are complex. Therefore, the rational GCQ rule can be further extended to more fading environments.

Finally, investigating how to find the poles of the rational functions used in the GCQ rule would possibly increase the accuracy of the calculations.

$$\sim$$

Bibliography

[1] J. G. Proakis and M. Salehi, *Digital Communications*. McGraw-Hill Education, 2007.

[2] Y. Dhungana and C. Tellambura, "Rational Gauss-Chebyshev quadratures for wireless performance analysis," *IEEE Wireless Commun. Lett.*, vol. 2, no. 2, pp. 215–218, 2013.

[3] A. Molisch, *Wireless Communications*. Wiley, 2010.

[4] *Mobile Communications - Data transmission in industry*. Phoneix Contact, 2012. [Online]. Available: https://www.phoenixcontact.com/assets/downloads_ed/global/web_dwl_technical_info/52000746_EN_DE_LR-1.pdf

[5] T. Halonen, R. Romero, J. Romero, and J. Melero, *GSM, GPRS and EDGE Performance: Evolution Towards 3G/UMTS*. Wiley, 2003.

[6] B. Li, D. Xie, S. Cheng, J. Chen, P. Zhang, W. Zhu, and B. Li, "Recent advances on TD-SCDMA in China," *IEEE Commun. Mag.*, vol. 43, no. 1, pp. 30–37, 2005.

[7] T. Okada, "Mobile terminal RF circuit technology for increasing capacity/coverage and international roaming," online, NTT DOCOMO, Tech. Rep., 2009. [Online]. Available: http://www.nttdocomo.co.jp/english/binary/pdf/corporate/technology/rd/technical_journal/bn/vol10_2/vol10_2_047en.pdf

[8] "IEEE standard for information technology–telecommunications and information exchange between systems local and metropolitan area networks–specific

requirements part 11: Wireless lan medium access control (MAC) and physical layer (PHY) specifications," *IEEE Std 802.11-2012 (Revision of IEEE Std 802.11-2007)*, pp. 1–2793, 2012.

[9] "IEEE standard for information technology - telecommunications and information exchange between systems - local and metropolitan area networks - specific requirements. - part 15.1: Wireless medium access control (MAC) and physical layer (PHY) specifications for wireless personal area networks (WPANs)," *IEEE Std 802.15.1-2005 (Revision of IEEE Std 802.15.1-2002)*, pp. 1–580, 2005.

[10] "The world in 2013: ICT facts and figures," online, ITU, Tech. Rep., 2013. [Online]. Available: http://www.itu.int/en/ITU-D/Statistics/Documents/facts/ ICTFactsFigures2013.pdf

[11] "Digtial cellular telecommunications system (Phase 2+); radio transmission and reception," online, GSM 05.05, Tech. Rep., Mar. 1996. [Online]. Available: http://www.etsi.org/deliver/etsi_gts/05/0505/05.00.00_60/gsmts_ 0505v050000p.pdf

[12] J. Liberti and T. Rappaport, "Accurate techniques to evaluate CDMA bit error rates in multipath channels with imperfect power control," in *Proc. IEEE Global Telecommun. Conf.*, 1995, pp. 33–37.

[13] "IEEE standard for local and metropolitan area networks: Overview and architecture. amendment 2: Registration of object identifiers," *IEEE Std 802-2001 (Revision of IEEE Std 802-1990)*, pp. 1–, 2002.

[14] "IEEE standard for local and metropolitan area networks part 16: Air interface for broadband wireless access systems," *IEEE Std 802.16-2009 (Revision of IEEE Std 802.16-2004)*, pp. 1–2080, 2009.

[15] C. Tellambura, Y. Dhungana, and M. Soysa, "Uniform approximations for wireless performance in fading, noise and interference," in *Proc. IEEE Int. Conf. Commun.*, 2012, pp. 2410–2415.

[16] Y. Dhungana and C. Tellambura, "Uniform approximations for wireless performance in fading channels," *IEEE Trans. Commun.*, vol. PP, no. 99, pp. 1–12, 2013.

[17] F. Xiong, *Digital Modulation Techniques*. Artech House, Incorporated, 2000.

[18] A. Annamalai and C. Tellambura, "A general approach for evaluating the outage probability in microcellular mobile radio systems," in *Proc. Int. Conf. Commun.*, vol. 3, 1999, pp. 1836–1840.

[19] M. K. Simon, *Digital Communication over Fading Channels*. Wiley, 2005.

[20] P. Borjesson and C. Sundberg, "Simple approximations of the error function $Q(x)$ for communications applications," *IEEE Trans. Commun.*, vol. 27, no. 3, pp. 639–643, 1979.

[21] N. Beaulieu, "A simple series for personal computer computation of the error function $Q(\cdot)$," *IEEE Trans. Commun.*, vol. 37, no. 9, pp. 989–991, 1989.

[22] M. Chiani and D. Dardari, "Improved exponential bounds and approximation for the Q-function with application to average error probability computation," in *Proc. IEEE Global Telecommun. Conf.*, vol. 2, 2002, pp. 1399–1402.

[23] M. Chiani, D. Dardari, and M. K. Simon, "New exponential bounds and approximations for the computation of error probability in fading channels," *IEEE Trans. Wireless Commun.*, vol. 2, no. 4, pp. 840–845, 2003.

[24] G. Karagiannidis and A. Lioumpas, "An improved approximation for the Gaussian Q-function," *IEEE Commun. Lett.*, vol. 11, no. 8, pp. 644–646, 2007.

[25] Y. Isukapalli and B. Rao, "An analytically tractable approximation for the Gaussian Q-function," *IEEE Commun. Lett.*, vol. 12, no. 9, pp. 669–671, 2008.

[26] W. M. Jang, "A simple upper bound of the Gaussian Q-function with closed-form error bound," *IEEE Commun. Lett.*, vol. 15, no. 2, pp. 157–159, 2011.

[27] Q. Shi and Y. Karasawa, "An accurate and efficient approximation to the Gaussian Q-function and its applications in performance analysis in Nakagami-m fading," *IEEE Commun. Lett.*, vol. 15, no. 5, pp. 479–481, 2011.

[28] O. Olabiyi and A. Annamalai, "Invertible exponential-type approximations for the Gaussian probability integral $Q(x)$ with applications," *IEEE Wireless Commun. Lett.*, vol. 1, no. 5, pp. 544–547, 2012.

[29] ——, "New exponential-type approximations for the $erfc(.)$ and $erfcp(.)$ functions with applications," in *Proc. Wireless Commun. and Mobile Computing Conf.*, 2012, pp. 1221–1226.

[30] G. T. F. De Abreu, "Arbitrarily tight upper and lower bounds on the Gaussian Q-function and related functions," in *Proc. Int. Conf. Commun.*, 2009, pp. 1–6.

[31] C. Tellambura and A. Annamalai, "Derivation of Craig's formula for Gaussian probability function," *Electron. Lett.*, vol. 35, no. 17, pp. 1424–1425, 1999.

[32] J. Stoer and R. Bulirsch, *Introduction to Numerical Analysis*. Springer-Verlag, 1980.

[33] E. Biglieri, G. Caire, G. Taricco, and J. Ventura-Traveset, "Simple method for evaluating error probabilities," *Electron. Lett.*, vol. 32, no. 3, pp. 191–192, 1996.

[34] ——, "Computing error probabilities over fading channels: A unified approach," *European Trans. Telecommun.*, vol. 9, no. 1, pp. 15–25, 1998.

[35] C. Tellambura, "Evaluation of the exact union bound for trellis-coded modulations over fading channels," *IEEE Trans. Commun.*, vol. 44, no. 12, pp. 1693–1699, 1996.

[36] E. Biglieri and G. Taricco, "Exact pairwise error probability of space-time codes," in *Proc. Int. Conf. Commun.*, vol. 3, 2002, pp. 1373–1376 vol.3.

[37] A. Annamalai, C. Tellambura, and V. Bhargava, "Efficient computation of MRC diversity performance in Nakagami fading channel with arbitrary parameters," *Electron. Lett.*, vol. 34, no. 12, pp. 1189–1190, 1998.

[38] ——, "Exact evaluation of maximal-ratio and equal-gain diversity receivers for M-ary QAM on Nakagami fading channels," *IEEE Trans. Commun.*, vol. 47, no. 9, pp. 1335–1344, 1999.

[39] M. Abramowitz and I. Stegun, *Handbook of Mathematical Functions: With Formulars, Graphs, and Mathematical Tables*. Dover Publications, Incorporated, 1964.

[40] J. V. Deun, A. Bultheel, and P. González-Vera, "On computing rational Gauss-Chebyshev quadrature formulas," *Math. Comput.*, vol. 75, no. 253, pp. 307–326, Oct. 2006.

[41] L. N. Trefethen, "Is Gauss quadrature better than clenshaw-curtis?" *SIAM Rev.*, vol. 50, no. 1, pp. 67–87, Feb. 2008.

[42] W. Gautschi, *Orthogonal Polynomials: Computation and Approximation*. Oxford University Press, 2004.

[43] F. Stetter, "Error bounds for Gauss-Chebyshev quadrature," *Mathematics of Computation*, vol. 22, no. 103, pp. 657–659, 1968.

[44] A. Annamalai, C. Tellambura, and V. Bhargava, "A general method for calculating error probabilities over fading channels," *IEEE Trans. Commun.*, vol. 53, no. 5, pp. 841–852, 2005.

[45] Z. Wang and G. Giannakis, "A simple and general parameterization quantifying performance in fading channels," *IEEE Trans. Commun.*, vol. 51, no. 8, pp. 1389–1398, 2003.

[46] A. Annamalai, C. Tellambura, and V. Bhargava, "Unified analysis of MPSK and MDPSK with diversity reception in different fading environments," *Electron. Lett.*, vol. 34, no. 16, pp. 1564–1565, Aug. 1998.

[47] A. Annamalai and C. Tellambura, "Error rates for Nakagami-m fading multichannel reception of binary and M-ary signals," *IEEE Trans. Commun.*, vol. 49, no. 1, pp. 58–68, 2001.

[48] P. Herath, U. Gunawardana, R. Liyanapathirana, and N. Rajatheva, "Outage probability analysis of multiple antenna dual-hop networks with interference-limited relay," *IEICE Trans. Commun.*, vol. E96-B, no. 2, pp. 577–584, 2013.

[49] C. Tellambura and A. Annamalai, "An unified numerical approach for computing the outage probability for mobile radio systems," *IEEE Commun. Lett.*, vol. 3, no. 4, pp. 97–99, 1999.

[50] M. J. Radermacher, "Probability of error analysis using a Gauss-Chebyshev quadrature rule," Master's thesis, Univ. of Colorado at Colorado Springs, 1999.

[51] M. Di Renzo, F. Graziosi, and F. Santucci, "Ei-transform: A useful and general framework for channel capacity analysis over fading channels," in *Proc. IEEE Sarnoff Symp.*, 2009, pp. 1–6.

[52] F. Yilmaz, O. Kucur, and M.-S. Alouini, "Exact capacity analysis of multihop transmission over amplify-and-forward relay fading channels," in *Proc. Int. Symp.*, 2010, pp. 2293–2298.

[53] K. Deckers, J. V. Deun, and A. Bultheel, "Rational Gauss-Chebyshev quadrature formulas for complex poles outside $[-1, 1]$." *Math. Comput.*, vol. 77, no. 262, pp. 967–983, 2008.

$\sim$